TOPICAL REVIEW

Vanadium-based nanowires for sodium-ion batteries

To cite this article: Yu Cheng *et al* 2019 *Nanotechnology* **30** 192001

View the article online for updates and enhancements.

IOP ebooks™

Bringing you innovative digital publishing with leading voices to create your essential collection of books in STEM research.

Start exploring the collection - download the first chapter of every title for free.

Topical Review

Vanadium-based nanowires for sodium-ion batteries

Yu Cheng, Yangyang Xia, Yiming Chen, Qin Liu, Tong Ge, Lin Xu[1] **and Liqiang Mai**[1]

State Key Laboratory of Advanced Technology for Materials Synthesis and Processing, International School of Materials Science and Engineering, Wuhan University of Technology, Wuhan 430070, People's Republic of China

E-mail: linxu@whut.edu.cn and mlq518@whut.edu.cn

CrossMark

Abstract

Sodium-ion batteries (SIBs) have received great attention because of the abundance source and low cost. To date, some Na^+ storage materials have achieved great performance, but the larger Na^+ radius and more complex Na^+ storage mechanism compared with Li^+ still limit the energy density and power density. This review systematically summarizes emerging synthetic technologies of vanadium-based materials from simple nanowires to complicated modified/ optimized structures. In addition, vanadium-based nanowire materials are reviewed at both the cathode and anode side, and advantages and drawbacks are proposed to explain the challenges facing application of novel materials. Furthermore, a vanadium-based single-nanowire device is reported to reveal the Na^+ storage mechanism, which contributes to the understanding of the reaction in SIBs. Finally, this review summarizes the current development challenges of SIBs and looks forward to the future development prospects of vanadium-based nanowires, providing a new direction for further applications of SIBs.

Keywords: vanadium, nanowires, sodium-ion batteries

(Some figures may appear in colour only in the online journal)

1. Introduction

With the rapid development of renewable energy, the shortage of energy resources and the environmental problems brought by fossil energy have attracted people's attention [1]. It is extremely important to develop new energy storage materials [2]. Lithium-ion batteries (LIBs) have become a popular renewable energy storage systems because of their high energy density, and have been widely used [3]. However, due to the limited supply of lithium on earth, it has not been able to meet the energy needs of people for a long time. Compared to lithium, the sodium resource is widespread and has also been applied in energy fields; the worldwide reserve of sodium is far higher than that of lithium [4, 5]. Hence,

sodium-ion batteries (SIBs) hold the absolute edge in large-scale production and application. In addition, because sodium and lithium share the same main group in the periodic table, they have lots of similarities in many aspects, such as a similar charge storage mechanism [6]. Therefore, on the basis of inheriting the excellent properties of lithium, SIBs have a promising prospect in the future market application and have already made a series of progressions in the energy storage field [4]. However, SIBs face inherent challenges in comparison to LIBs, such as lower voltage, poorer cycling stability, and a smaller diffusion coefficient [6]. Moreover, because of the larger ionic size of Na^+, the influence on the electrode crystal structure during sodium-ion intercalation/ deintercalation leads to severe degradation of the electrodes [5, 7]. In addition, the higher electrochemical potential ($\sim$0.3 V versus Li^+/Li) and higher mass of sodium leads to

lower energy density of SIBs, which greatly limits their development [8]. Therefore, the most vital task is to find a suitable electrode material, which contributes to the advancement of specific capacity and cycling stability.

Due to the joint efforts of researchers all over the world, a series of high capacity electrode materials have been fabricated in the study of SIBs. However, they are still far from industrial application due to the significant collapse of materials during cycling caused by the larger Na^+ radius. To solve this issue, researchers began to study the modification of electrode materials on the structures, while the types of electrode materials have been studied almost completely. According to recent research, one-dimensional (1D) nanostructures, especially nanowires, have special superiorities. Firstly, nanowires provide a shorter ion diffusion length because of the ~100 nm width, which has the potential to increase the rate performance [9]. Secondly, the high surface area of nanowires offers more electrolyte–electrode contact area and reduced charging/discharging time [3, 10]. Thirdly, the interlaced structure constructed by nanowires can buffer the external stress and promote the internal stress dispersion [11], which can adjust to the volume expansion and restrain the mechanical degradation to some extent. However, the improvements in nanostructures cannot fundamentally solve the problem of volume expansion [9]. Therefore, the intrinsic electrochemical stability of the material is also critical to the development of batteries. In terms of the electrode materials in SIBs, phosphate-based compounds are the most promising cathode materials due to the fast Na^+ transmission rate, but they possess low capacity. Hard carbon is widely used as an anode material, however, poor cycling stability limits its application [12]. The development of SIBs is constrained by the mediocre performance of current electrode materials. Vanadium-based materials have attracted more attention because of the low price and abundant source, and have already made a great contribution to SIBs due to the advantage of high specific capacity (the single-crystalline bilayered V_2O_5 nanobelts can deliver a high capacity of 229 mA h g^{-1} at 80 mA g^{-1} as the cathode) [13]. In addition, they also have good performance as anode materials; it has been reported that V_2O_3 is one new selective insertion and multiphase conversion type anode material with a high capacity of SIBs (165 mA h g^{-1} at 20 A g^{-1}) [14]. All the valence electrons of the V atom can take part in bonding, thereby giving rise to a multivalent V from V^{2+} to V^{5+}, resulting in strong V–O bond strength and various structures [8]. Furthermore, as for the insertion-type vanadium-based electrode, the volume change under low voltage would be less than that of the representative conversion-based materials, which means superior cycling stability [15]. Recently, vanadium-based materials have been widely used in energy storage systems, such as SIBs [16], zinc-ion batteries [17], magnesium-based batteries [18], etc. Therefore, to improve the electrode materials of SIBs, more investigations have focused on vanadium-based materials. For example, a vanadium oxide electrode (especially layered vanadium oxide, such as VO_2 and V_2O_5), which has been studied in LIBs and shows initial capacities above 300 mA h g^{-1} [7], also exhibits great properties during

the cycling of SIBs [19, 20]. A vanadium sulfide electrode (such as VS_4 [21] and V_5S_8 [22]) is conducive to the conveyance of electron/ionic charge carriers and the improvement of capacity and stability because it offers not only electronic properties but also adequate space to host Na^+ [21, 22]. Moreover, the vanadium-based phosphates (such as $Na_3V_2(PO_4)_3$) can also improve the structure and cycling stability, even at high charge states. Hence, vanadium-based nanowires have promising prospects in SIBs [23].

Herein, we introduce the design and synthesis of vanadium-based nanowires from different structures, including simple, porous, core–shell/coated, arrays, and network/membrane structures. In addition, this review also summarizes the applications of vanadium-based nanowires in SIBs according to different classifications, including cathode, anode, and single-nanowire devices. Finally, based on the present results of research, we put forward some views on the development prospects of vanadium-based nanowires in SIBs.

2. Design and synthesis

The structures and properties of nanowires could be regulated by various synthesis strategies. Particularly, numerous studies have demonstrated that the design and synthesis of nanowires have a significant influence on the electrochemical performance in energy storage applications. The design and synthesis include nanowire growth mechanisms and controllable synthesis in terms of dimensions, morphology, composition, alignment, and their compounds. It is important to develop various techniques to control the morphology, stable crystal structure, uniform shape and size of 1D nanostructures [24]. Vanadium-based nanowires are considered as promising materials due to their high specific capacity and high energy density, and have been widely employed in numerous energy storage applications. Nowadays, the rapid development of nanotechnology has significantly accelerated the energy storage field to explore novel stable materials with great electrochemistry performance. Here, we focus on the vanadium-based nanowires, which could be designed and synthesized to various structures, such as simple nanowires, porous nanowires, core–shell/coated nanowires, nanowire arrays, and nanowire networks/membranes. We introduce the great contribution of these unique structures in energy storage systems and some of their achievements in SIBs are highlighted to emphasize the importance of special structures. In addition, their synthetic methods are reported in detail. Some of the representative examples are listed in table 1.
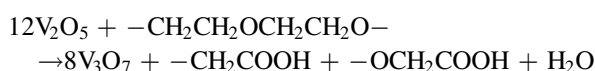
2.1. Simple nanowires

As an emerging material applied in the energy field, nanomaterial has received extensive attention from many scholars [25]. With the aim of improving its physical and chemical properties, various experimental methods have been summarized on surface modification and structural regulation [26]. Among these studies, the synthesis and application of 1D nanowire materials are undoubtedly promising research

Table 1. Morphology/structure of nanowire electrodes for SIBs.

Morphology/ structure	Material	Synthesis strategy	Applications	Typical performance	Ref
Simple nanowires	α-V_2O_5	Liquid phase methods	Cathode	30 mAh g^{-1} at 20 mA g^{-1}	[27]
	VO_2	Liquid phase methods	Cathode	55 mA h g^{-1}	[107]
	β-$Na_{0.33}V_2O_5$	Liquid phase methods	Cathode	90 mA h g^{-1} at 20 mA g^{-1}	[27]
	$Na_{1.25}V_3O_8$	Liquid phase methods	Cathode	69.3 mA h g^{-1} at 200 mA g^{-1}	[6]
	$Na_xV_2O_5$	Liquid phase methods	Cathode	365 mA h g^{-1} at 20 mA g^{-1}	[28]
	$Na_3V_2(PO_4)_3$	Liquid phase methods	Cathode	19.1 mA h g^{-1} after 50 cycles at 1 C	[29]
Porous nanowires	Graphene–$FePO_4$	Liquid phase methods	Cathode	124.2 mA h g^{-1} at 0.5 C	[43]
	CuO	Liquid phase methods	Anode	303 mA h g^{-1} after 50 cycles at 50 mA g^{-1}	[44]
Core–shell/coated nanowires	$Na_3V_2O_2(PO_4)_2F/RuO_2$	Liquid phase methods	Cathode	95 mA h g^{-1} at 20 C	[48]
	VO_2/C	Liquid phase methods	Cathode	328 mA h g^{-1} at 0.3 C	[49]
	$NaV_3(PO_4)_3/C$	Electrospinning methods	Anode	118 mA h g^{-1} at 1 C	[65]
Nanowire arrays	$Na_3(VO)_2(PO_4)_2F$	Liquid phase methods	Cathode	130 mA h g^{-1} at 0.5 C	[56]
	$Na_2Ti_2O_5$-VS_2	Liquid phase methods	Cathode	203 mA h g^{-1} at 1 C	[57]
	V_2O_5/C	Liquid phase methods	Cathode	93 mA h g^{-1} at 1 A g^{-1}	[58]
	$V_2O_3/CNTs$	Liquid phase methods/ chemical deposit methods	Cathode	612 mA h g^{-1} at 0.1 A g^{-1}	[59]
Nanowire networks/ membranes	$V_2O_5 \cdot nH_2O$	Liquid phase methods	Cathode	96 mA h g^{-1} at 1.0 A g^{-1}	[20]
	$Na_3V_2(PO_4)_3$	Template-assisted methods	Cathode	94 mA h g^{-1} at 100 C	[65]
	$H_2V_3O_8$	Liquid phase methods	Cathode	168 mA h g^{-1} at 10 mA g^{-1}	[19]
	V_2O_5/CNT	Liquid phase methods	Anode	80% of the initial capacity after 900 cycles at 60 C	[66]
	$V_2O_3 \subset$ C-NTs $\subset$ rGO	Liquid phase methods	Anode	165 mA h g^{-1} at 20 A g^{-1}	[14]

directions in the field of nanomaterials [9]. In fact, vanadium oxides are used in various applications because of their versatile redox-dependent properties [3]. The 1D morphology is useful for many applications and therefore a variety of methods are fabricated, such as hydrothermal/solvothermal synthesis, electrospinning, and surfactant-assisted solution to synthesize 1D vanadium nanostructures [24, 27–29]. Ultralong $H_2V_3O_8$ nanowires were synthesized by Mai's group with excellent electrochemical properties [18, 30, 31]. Firstly, The V_2O_5 powder was melted at high temperature and added to deionized water to form a sol [32]. Then, ultralong $H_2V_3O_8$ nanowires based on the V_2O_5 sol were achieved by a hydrothermal method. At the beginning of the reaction, polyethylene glycol-4000 (PEG-4000) has an inductive effect that causes the electron cloud to move toward the oxygen atoms in the PEG-4000 based on the theory of electronegativity. Therefore, the V_2O_5 sol would wrap around the PEG-4000 by an electrostatic effect. As the reaction proceeded, oxidation–reduction of vanadium pentoxide with aniline and PEG-4000 took place and generated polyaniline. The redox reaction was described as follows.

$$12V_2O_5 + -CH_2CH_2OCH_2CH_2O-$$
$$\rightarrow 8V_3O_7 + -CH_2COOH + -OCH_2COOH + H_2O$$

By the electrostatic repulsion of polyoxovanadate clusters, polymer clusters were arranged in parallel to reduce the

system energy. Finally, ultralong $H_2V_3O_8$ nanowires were obtained. With a unique 1D structure, this material displays high specific reversible capacity and excellent cycling stability (figures 1(a), (b)). Modified 1D vanadium-based nanowires have also been studied. Silver vanadium oxide nanowires were obtained by Xiong *et al* via a hydrothermal method [33], and were applied in electrochromic devices and showed excellent performance. On the other hand, electrospinning is a special fiber manufacturing approach in which a polymer solution or melt is sprayed in a strong electric field, and which has also been applied in the synthesis of nanowires by Mai *et al* [34]. Under the effect of the electric field, the droplets at the needle will change from a spherical shape to a conical shape, and the fiber filaments will be extended from the conical tip. And in the ultralong nanowire structures prepared by electrospinning technology, nanorods will be attached to ultralong nanowires. In addition to the above two main methods, some other methods are also applied in the synthesis of nanowires. The chemical vapor deposition (CVD) method was used by Peng *et al* to obtain single-crystal VO_2 nanowires [35]. The V_2O_5 was selected as the only precursor and was decomposed in a tube furnace, and the nanowires grew on the quartz substrates (figures 1(c), (d)). At the same time, it was found that the partial pressure of oxygen during the growth process will affect the type and amount of carriers inside the materials. Many different kinds of
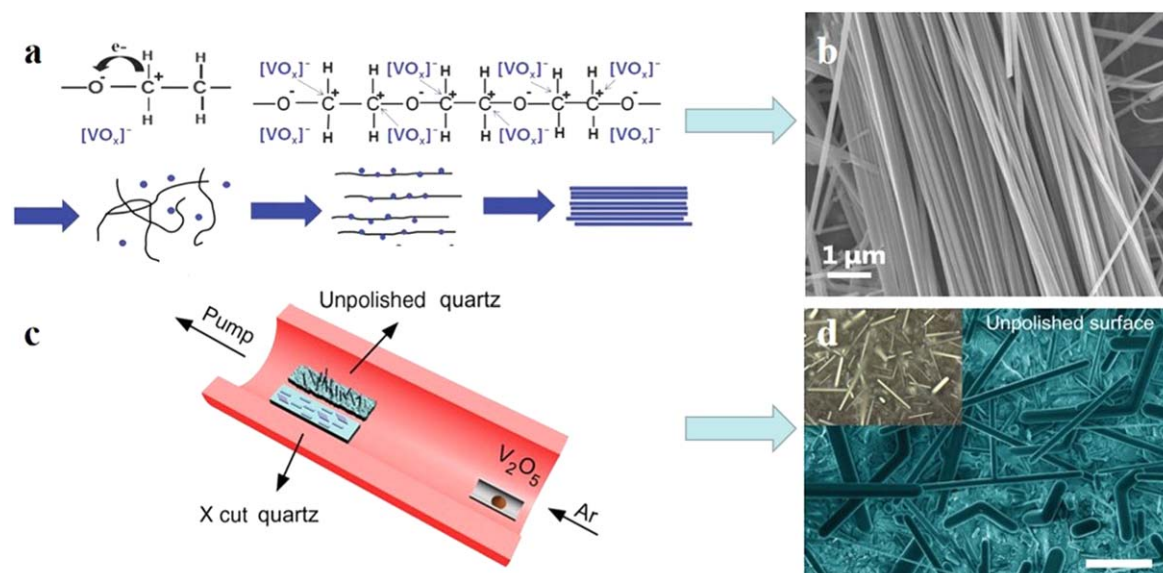
Figure 1. (a) A schematic illustration of the formation of bunched $H_2V_3O_8$ nanowires. (b) Scanning electron microscopy (SEM) images of the bunched $H_2V_3O_8$ nanowires. Reproduced from [31] with permission of The Royal Society of Chemistry. (c) A schematic drawing of the CVD setup. (d) An SEM image of the VO_2 nanowires on an unpolished quartz substrate. Scale bar: 4 μm. Inset: an optical microscope image of the same substrate showing free-standing nanowires. Reproduced figure with permission from [35]. Copyright 2016 by the American Physical Society.

vanadium-based nanowires have been synthesized by the above methods, such as $H_2V_3O_8$ nanowires, VO_2 nanowires, silver vanadium oxide nanowires, and so on. The ideal 1D nanostructures need to have properties of the same shape, uniform size, perfect crystal structure, no morphological defects, and uniform composition.

2.2. Porous nanowires

Generally speaking, the structures of simple nanowires cannot meet the electrochemical requirements. Among them, some materials need further modification to overcome the original drawbacks, including poor conductivity and serious volume expansion during the cycling. We introduce some typical methods to modify the morphology of nanowires and obtain excellent properties [9]. Compared to simple nanowires, the structures of porous nanowires are more diverse. Porous nanowires create interior void spaces, which provide a large specific surface area and more reactive sites. After many years of research and exploration, porous nanowires with adjustable pore sizes, variable composition, and different pore structures have been synthesized. Owing to this unique structure, the battery has a longer cycle life, a larger specific capacitance, and a higher efficiency of charge and discharge. At the same time, the excellent pore structure makes the ion diffusion rate and electron conduction rate increase. A variety of 1D porous nanowire structures have been constructed by combining the advantages of 1D nanoarchitectures and porous structures, which would be widely used in the energy storage field [36]. Zhang *et al* utilized an NH_4VO_3 acidic solution as the vanadium precursor to obtain $NH_4V_3O_8$ nanowires via a hydrothermal method [37]. The $NH_4V_3O_8$ nanowires possessed interconnected pore networks via an annealing

treatment, which made the $NH_4V_3O_8$ nanowires break down and begin to produce N_2. As the pressure increased, the unique open pore structure began to form. Finally, the mesoporous VO_2 nanowires were achieved. The composite structure of nanowires and mesopores offers more active sites, which may improve the electrochemical performance (figures 2(a)–(c)). The top-down method is applied in the regulation of pore structure in nanowires, which provides the material with excellent rate capability and stable capacity [38]. The hydrothermal method is widely used because of its simple operation. To improve the electrochemical stability of vanadium nitride (VN), which is a highly valuable electrode material for asymmetric supercapacitors, Lu *et al* synthesized vanadium oxide (VO_x) nanowires by the hydrothermal method [39]. Also, VN nanowires were obtained by annealing the as-prepared VO_x nanowires. The asymmetric supercapacitors based on the VN nanowire anode and the VO_x nanowire cathode displayed excellent electrochemical performance. In addition, some scholars are also exploring the application of porous vanadium-based nanowires in flexible all-solid-state supercapacitors. Mesoporous VN nanowires (MVNNs) were fabricated by Xiao *et al* via hydrothermal synthesis and subsequent thermal nitridation under an NH_3 atmosphere [40]. And they were used to assemble MVNN/ carbon nanotube (CNT) hybrid electrodes whose unique pore structure accelerates the ion diffusion rate and electron conduction rate in flexible all-solid-state supercapacitors. On the other hand, porous nanowires have also been obtained by electrospinning technology. Li *et al* successfully applied electrospinning technology and annealing to achieve porous vanadium pentoxide 1D material [41]. By controlling an appropriate annealing time and temperature, the partial organic functional group will be retained, which will improve
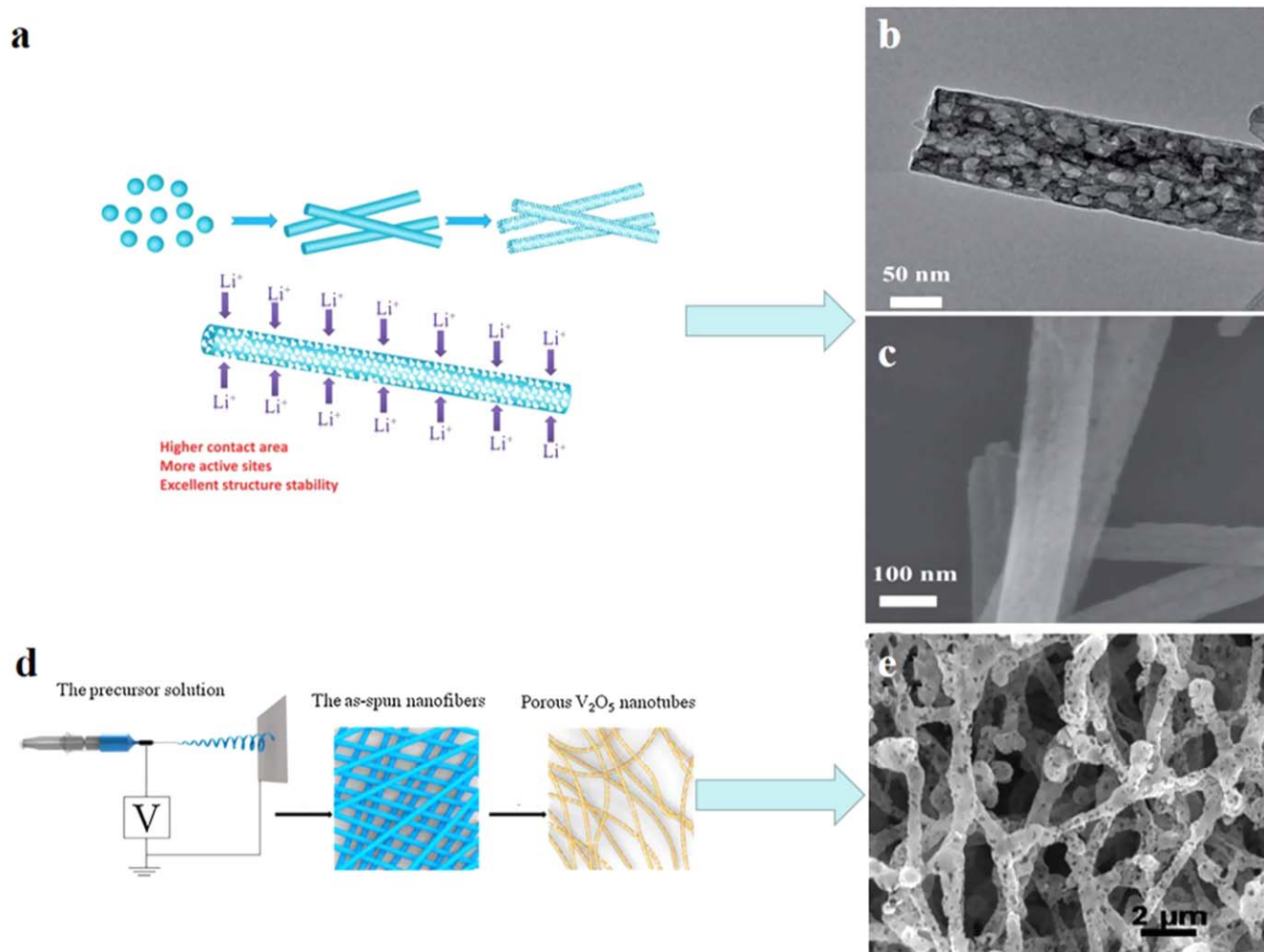
Figure 2. (a) Schematic illustration of the fabrication steps and proposed formation mechanism of the mesoporous nanowires and mesoporous nanowires offering high contact area, more active sites, and excellent structural stability during lithium insertion/deinsertion. (b) A transmission electron microscopy (TEM) image of mesoporous VO_2 nanowires. (c) An SEM image of mesoporous VO_2 nanowires. Reproduced from [37] with permission of The Royal Society of Chemistry. (d) Electrospinning preparation of porous V_2O_5 1D material: electrospinning process; annealing process. (e) SEM images of nanostructures of V_2O_5. Reprinted from [41], Copyright 2015, with permission from Elsevier.

the electronic conductivity of the material. These porous vanadium pentoxide nanowires with residual organic ligands possess superior electrochemical stability and high rate performance in LIBs (figures 2(d), (e)). In summary, obtaining precursors of porous vanadium-based nanowires by the hydrothermal method is the first step in the synthetic pathway. Annealing or calcination is then performed to form a porous structure. The hydrothermal method has been widely used in the synthesis of nanowires, and it is easy to operate. But it is hard to precisely control the nanowire structure. Moreover, electrospinning technology is also used for obtaining porous vanadium-based nanowires. It is conducive to the regulation of the nanowire structure, which gives the materials the advantages of small pore size and high porosity. Each method has its own advantages and disadvantages and needs to be selected according to specific conditions. In short, since the pores at the surface provide high contact area between the electrode materials and electrolyte, excellent ion transport capability is achieved [42]. Porous vanadium-based

nanowires demonstrate great performance in LIBs and supercapacitors, and this porous structure also provides good improvement in SIBs [43, 44]. Hence, porous vanadium-based nanowires could become promising electrode materials for SIBs.

2.3. Core–shell/coated nanowires

Although the porous structures can increase the lithium-ion transmission rate, the poor electrical conductivity of some materials has still not been solved. In addition, only one material cannot completely solve the problem of volume expansion during the cycling [11]. Effective surface modification and bonding of different materials can significantly inhibit structural degradation caused by volume expansion. The surface structures provide a buffer for electrode material change [45]. Moreover, the specific surface area of the electrode material can be increased by designing its structure to accelerate the ion transfer rate and increase the reaction sites

[46]. Hence, tremendous efforts have been devoted to investigating new types of coating structures. Typical examples of these strategies are introduced in this section, including CVD, physical vapor deposition (PVD), sol–gel, self-assembly, electrodeposition, etc. Novel cucumber-like heterostructure nanowires were synthesized by Mai *et al*. The V_2O_5 nanowires were coated with PEDOT with enriched MnO_2 nanoparticles; this heterostructure delivers mechanical integrity and inhibits excessive volume expansion after cycling, which effectively enhances the electrochemical performance [47]. Peng *et al* used ruthenium oxide to coat vanadium fluorophosphate nanowires and obtained excellent performance[48]. The reaction mechanism of $Na_3V_2O_2(PO_4)_2F$ with diameters of several tens of nanometers was investigated and the poor electrochemical properties of $Na_3V_2O_2(PO_4)_2F$, because of the large particles and low intrinsic conductivity, were solved (figures 3(d)–(h)). The preparation process is as follows: anhydrous $RuCl_3$ was dissolved in deionized water to form a stable black solution; then, the black $RuCl_3$ solution was added to the $Na_3V_2O_2(PO_4)_2F$ suspension at a steady uniform rate. The black suspensions were filtered into black powder and washed with anhydrous ethanol and deionized water several times. Finally, the black suspensions were dried at $150\,^{\circ}C$ for $20\,h$. The reversible capacitance of this material can reach $120\,mA\,h$ g^{-1} at $1\,C$ and $95\,mA\,h\,g^{-1}$ at $20\,C$ after 1000 cycles.

Just like Peng, Balogun *et al* also used a hydrothermal method to fabricate a novel method of coated VO_2 interleaved nanowires with carbon quantum dots (C-VOCQDs) [49], which solved the complexity of nanometer-modified VO_2 based electrodes (figures 3(a)–(c)). They grew $C-VO_X$ on a three-dimensional (3D) exposed carbon cloth by a hydrothermal method (VO_X nanowires with diameters between hundreds of nanometers uniformly coated on carbon cloth (C-VO)). The C-VOCQD was obtained by soaking the C-VO sample in carbon quantum dot (CQD) solution for $6\,h$. The synthesized material has great flexibility and can improve the storage capacity of sodium ions, which delivers a high initial capacity ($173\,mA\,h\,g^{-1}$) at $60\,C$, and the initial capacity of 80% can still be obtained by circulating 200 cycles. The special triaxial silver vanadium oxides/polyaniline (SVO/PANI) nanowires were successfully synthesized via *in situ* chemical oxidation polymerization and interfacial redox reaction by the Mai group [50]. Firstly, after adding an aniline monomer into a $AgVO_3$ solution, the monomer was uniformly dispersed on the surface of $AgVO_3$ nanowires. Then, part of the Ag^+ on the nanowires was dissolved and oxidized with aniline monomer to form an intermediate layer. Finally, triaxial nanowires were obtained by adding ammonium persulfate to form a PANI layer (figure 4).

A previous study once reported a carambola-shaped VO_2 nanostructure as a binder-free electrode for aqueous Na-air batteries, which shows high cycle efficiency and cycling stability up to 50 cycles. This VO_2 nanostructure was also used for the first time as an electrochemical catalyst for metal-air batteries, and exhibited high theoretical capacity, rapid ion diffusion rate, and low cost as an electrode material for metal-ion batteries. In addition, the synthesis of carambola-shaped VO_2 nanostructures on reduced graphene oxide (rGO) coated carbon paper was achieved via a simple hydrothermal method, but it efficiently avoided hindering the ion/electron transport and corroding the carbon electrode, caused by adding binder to the slurry. Hence, this 3D carambola-shaped VO_2 nanostructure is a promising catalytic material instead of the binder [51]. In general, compared with other structures, nanocomposite coatings have excellent stability and electrochemical performance, and the preparation method is relatively simple. It is believed that the application of nanosurface coatings will be widespread in many fields due to the continuous progress in the preparation and synthesis of nanomaterials.

2.4. Nanowire arrays

Compared with 1D simple nanowire structures, nanowire arrays improve the nonadjustable specific surface area and porosity of 1D structures because of the following properties [52]: (1) there is a gap between each nanowire of the nanowire arrays. These spaces can provide a direct channel between the electrode and electrolyte so that every single-nanowire can participate in the reaction; (2) there are larger contact areas between the electrode and electrolyte, which means more reaction points; (3) the nanowire arrays can grow directly on the collector, and the short ion transport distance reduces the transport resistance of ions in the solid; and (4) the gap between the arrays allows the change in the electrode volume during the intercalation of the ions, which ensures the stability of the cell. This special structure can improve the storage capacity, rate capacity and power density of the electrode, and prolong the cycle life of the electrode. In addition, the use of additives is another advantage that enables the preparation process to be simplified [53–55]. Two main basic strategies were used to synthesize nanowire arrays: top-down and bottom-up approaches. In the top-down approach, the desired structure could be constructed by transforming the crystal using traditional lithography, cutting, grinding, etching, etc. The bottom-up approach constructs a complicated crystal structure by individual atom and molecule self-assembly, which relies on the chemical properties of the material. Chao *et al* prepared $Na_3(VO)_2(PO_4)_2F$ (NVOPF) arrays on a graphene foam skeleton by a two-step solvothermal method [56]. This kind of 3D electrode structure is very helpful to shorten ion transport channels, enhancing energy density and cycle life. In this paper, the authors first deposited the seed layer of VO_2 nanoparticles on a 3D graphene foam skeleton during the first step of the solvothermal process. In the second step, the nanoparticles were transformed into NVOPF nanorods. As the reaction proceeds, a rectangular NVOPF array grows vertically on a hollow graphene skeleton. The working rate and energy density of the assembled Na^+ mixed energy storage device can reach $20\,C$ and $215\,W\,h\,kg^{-1}$ (figure 5).

Liao *et al* [57] synthesized nanowire arrays of $Na_2Ti_2O_5$ (NTO) coated with VS_2 nanosheets by a hydrothermal
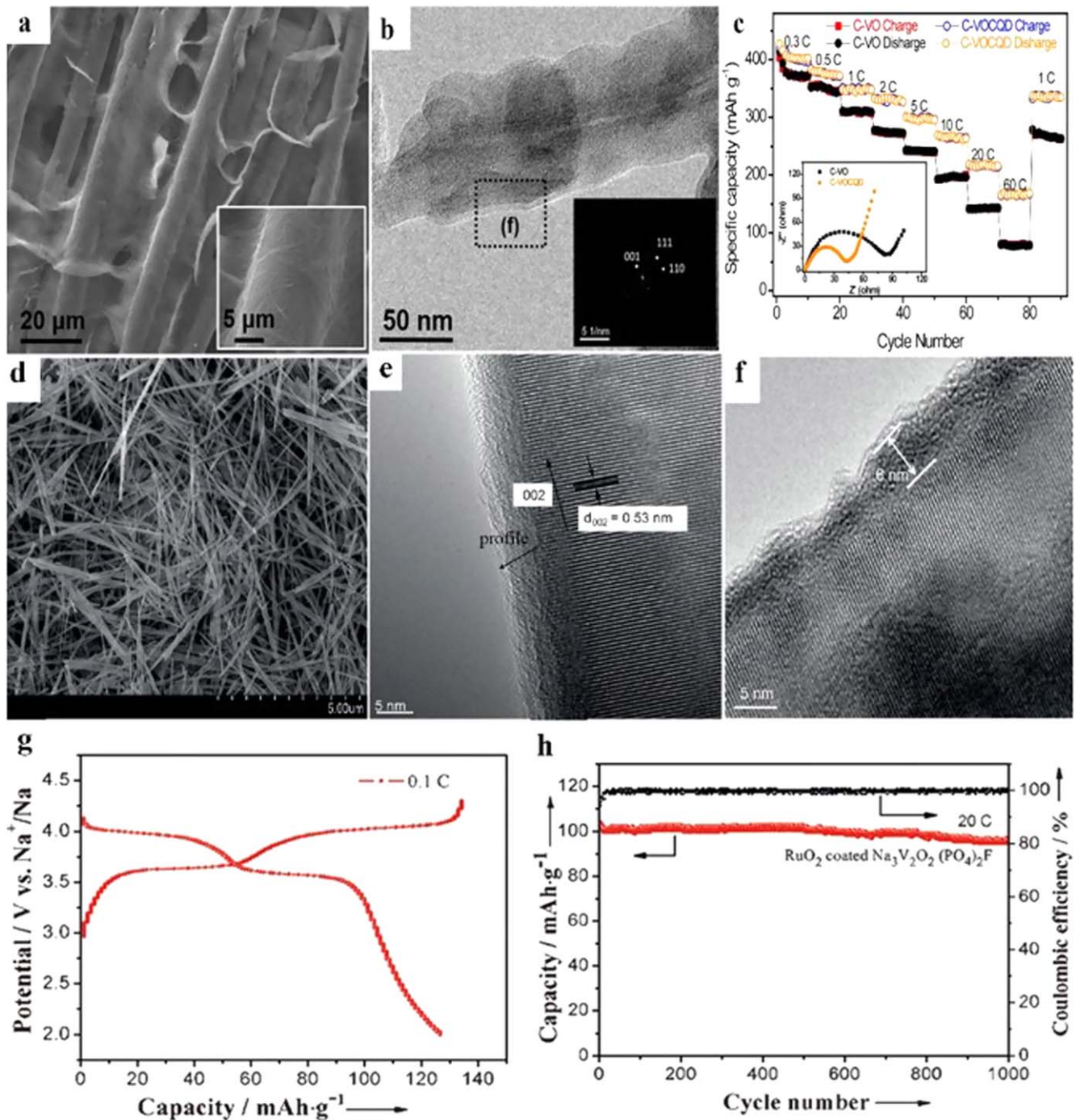
Figure 3. (a) SEM images of the C-VOCQD. (b) A TEM image of a single C-VOCQD nanowire. (c) Rate capability of the C-VO and C-VOCQD electrodes. (Inset is the Nyquist plots at fully charged stage). Reprinted with permission from [49], Copyright 2016 American Chemical Society. (d) SEM images of $Na_3V_2O_2(PO_4)_2F$ nanowires with space groupI4/mmm at low magnification (X10000). (e) A high resolution TEM (HRTEM) image of the $Na_3V_2O_2(PO_4)_2F$ nanowires. (f) A HRTEM image of the RuO_2-coated $Na_3V_2O_2(PO_4)_2F$ nanowires with a 6 nm RuO_2 layer. (g) Charge and discharge profiles of RuO_2-coated $Na_3V_2O_2(PO_4)_2F$ nanowires at a current density of 0.1 C in the voltage range of 2.5–4.3 V versus Na^+/Na. (h) Long-term cycling performance of the RuO_2-coated $Na_3V_2O_2(PO_4)_2F$ nanowires at a current density of 20 C. [48] John Wiley & Sons. © 2015 WILEY-VCH Verlag GmbH & Co. KGaA, Weinheim.

method. This type of structure can solve the problem of the low capacity of sodium titanate in SIBs due to the large interlayer spacing of VS_2 (figures 6(a)–(d)). Firstly, titanium foils coated with the $Na_2Ti_2O_5 \cdot H_2O$ nanowires were soaked in HCl for 3 h to form $H_2Ti_2O_5 \cdot H_2O$ nanowire arrays, and the titanium foil was removed from the HCl solution. After

the nanowire arrays were immersed in NaOH, the nanowire arrays were calcined at 600 °C for 3 h to obtain the $Na_2Ti_2O_5$ nanowire arrays. Finally, the nanowire arrays were coated with VS_2 to obtain the NTO-VS_2 arrays. After 100 cycles at 1 C, the capacity of the NTO-VS_2 remains at 203 mA h g^{-1}. Wang *et al* [58] synthesized various shapes of V_2O_5,
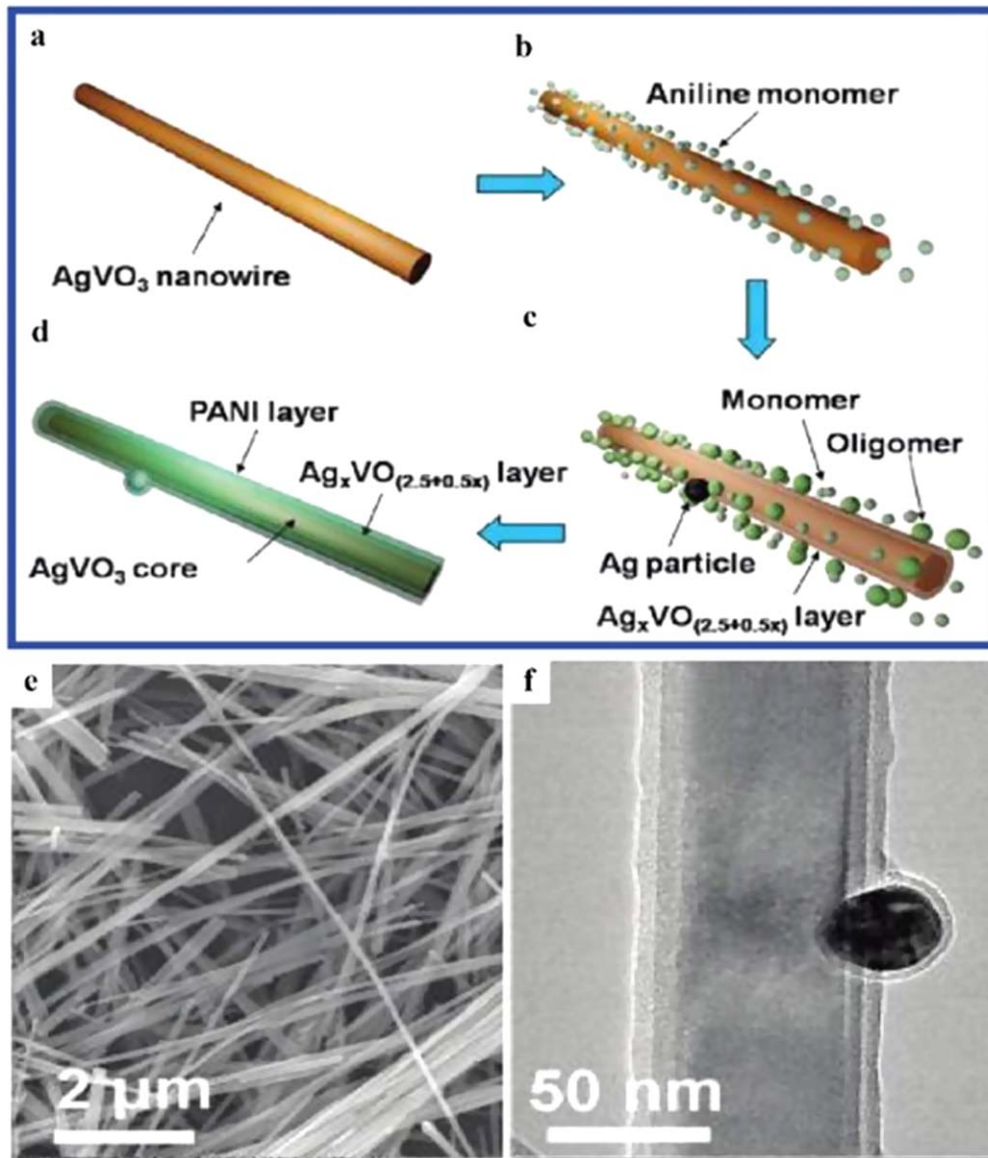
Figure 4. (a)–(d) A schematic illustration of the formation of SVO/PANI triaxial nanowire. (e) Field emission scanning electron microscope (FESEM) images of β-AgVO$_3$ nanowires and triaxial nanowires. (f) TEM images of SVO/PANI triaxial nanowires. Reprinted with permission from [50]. Copyright 2011 American Chemical Society.
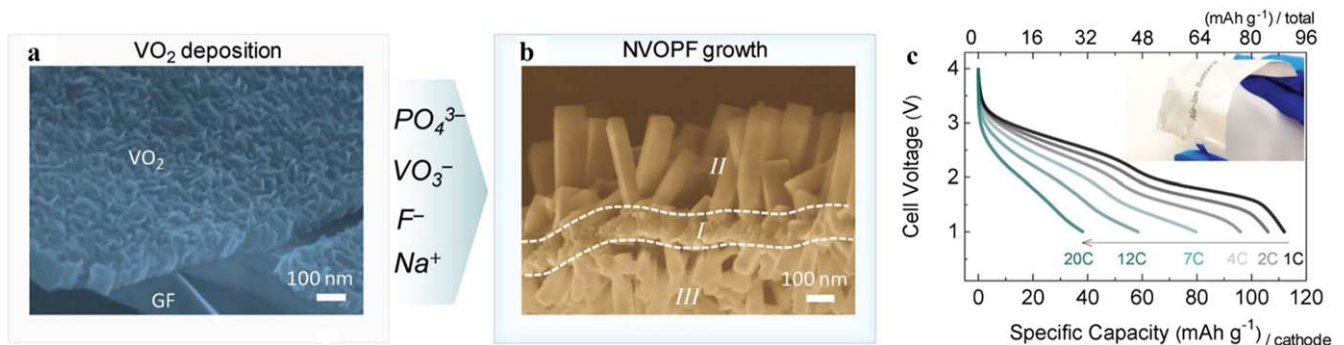

Figure 5. The synthesis strategy and microstructure of the graphene foam (GF) supported NVOPF nano-array. (a), (b) Cross-section FESEM images for the GF-VO$_2$ nanosheet seed layer precursor and GF-NVOPF array electrode. (c) Galvanostatic charge/discharge profiles from 1 to 20 C between 1 and 4 V (1 C is defined as 130 mA g^{-1}). The inset is the flexibility demonstration of the assembled soft-packed pouch cell. Reprinted with permission from [56]. John Wiley & Sons. © 2018 WILEY-VCH Verlag GmbH & Co. KGaA, Weinheim.
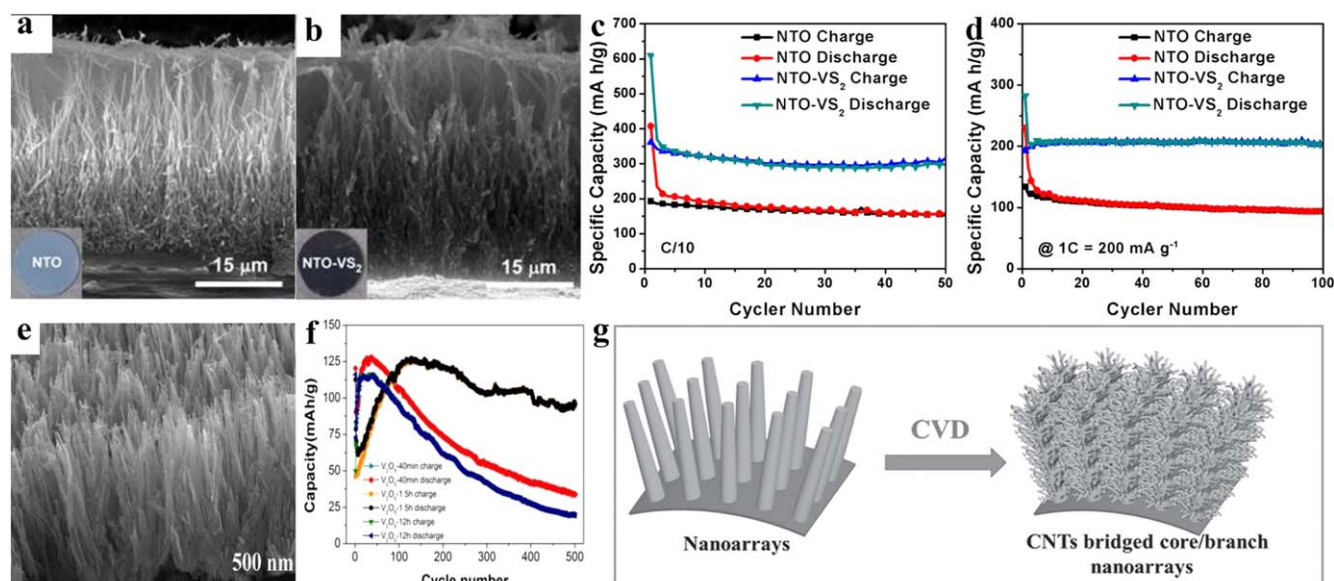
Figure 6. (a) SEM images of NTO. (b) SEM images of NTO-VS$_2$ nanowires. (c) Cycling performance comparison of NTO and NTO-VS$_2$ electrodes at C/10 rates and (d) 1 C rates. Reprinted from [57]. Copyright 2015, with permission from Elsevier. (e) Side-view SEM images of V$_2$O$_5$ arrays on Ti foil at the reaction time of 1.5 h. (f) Cycling of V$_2$O$_5$ at a current of 0.25 A g^{-1} at different reaction times. Reprinted from [58], Copyright 2015, with permission from Elsevier. Schematics of the CNT-bridged core/branch arrays electrode structure. (g) CVD growth of interwoven CNT branches on the surface of preformed metal oxide arrays (e.g. nanotubes, nanowires, nanoflakes, microrods). [59] John Wiley & Sons. © 2016 WILEY-VCH Verlag GmbH & Co. KGaA, Weinheim.

including V$_2$O$_5$ arrays on conductive titanium foil, by using a simple hydrothermal method (figures 6(e), (f)). By tightly joining the prepared materials to the substrate without the use of adhesives, a strong bond relationship was established between the two, which solved the adverse effect of electron transport between electrode and collector during charge and discharge. The general synthetic process is as follows: mixing NH$_4$VO$_3$ and H$_2$C$_2$O$_4$ · 2H$_2$O in deionized water. Then, magnetic stirring for 15 min to obtain a yellowish green solution, calcined in the reactor. The samples were washed and dried with distilled water several times. Finally, the V$_2$O$_5$ nanowire arrays were obtained by sintering at 500 °C in air. Among all shapes, the V$_2$O$_5$ arrays have the best cycling performance (95 mA h g^{-1} after 500 cycles). Xia *et al* studied the branching synthesis of CNTs on different metal oxide arrays and proposed a general synthetic method of CNT-bridged metal oxide core/branch arrays [59]. Metal oxide nanoarrays were prepared on different substrates by simple hydrothermal, CVD, or other solution methods (figure 6(g)). Then, CNTs were grown on the surface at 600 °C. The core/branched electrode with CNTs has the following advantages: (1) a comprehensive conductive network structure with horizontal and vertical conduction paths; (2) a high porosity and large specific surface area; and (3) a stable nanostructure. VO$_2$ is a material with high capacity but poor stability. Chao *et al* designed a novel non-adhesive cathode for high-performance batteries [55]. VO$_2$ arrays grew directly on a graphene network by the bottom-up type. In addition, fast ion diffusion caused by VO$_2$ nanobelts and the coated graphene quantum dots can significantly improve the cycling stability. Therefore, the modification of a nanostructured surface ensures excellent electrochemical performance.

In summary, nanowire arrays are synthesized from monomers by chemical polymerization or other methods and the formation of synthesized nanowire arrays can be controlled by kinetics. Several methods of synthesizing nanowire arrays have been introduced, and it has been proved that the composition and the geometry of the nanowire arrays can be tuned at high resolution for different energy storage applications. Hence, the above-mentioned nanowire arrays are considered as an ideal structure for electrode materials in energy storage systems.

2.5. Nanowire networks/membranes

Compared with the low-dimensional structures, the 3D network or membrane structures based on 1D nanowires have a highly specific surface area, which can provide a larger interface for the reaction of the material [60]. Moreover, the 3D network/membrane structures are more stable, which can effectively prevent aggregation and pulverization of the nanomaterials [61]. Three-dimensional reticular structures are usually characterized by disordered macroporous structures and laminated two-dimensional (2D) structures, which have specific properties in different length sizes, such as light weight, large specific surface area and high porosity. These structures have been widely used in 2D systems: the most typical feature is the porous network of graphene and its derivatives. Moreover, the interpenetrating network nanowire structures have a stable layered structure, fast ion channels, and 3D electron transport networks; they can also avoid the agglomeration of nanowire structures in charge and discharge. Thus, these network structures have great potential in electrochemical energy storage devices [19]. Recently, considerable efforts have been devoted to fabricating new types of 3D
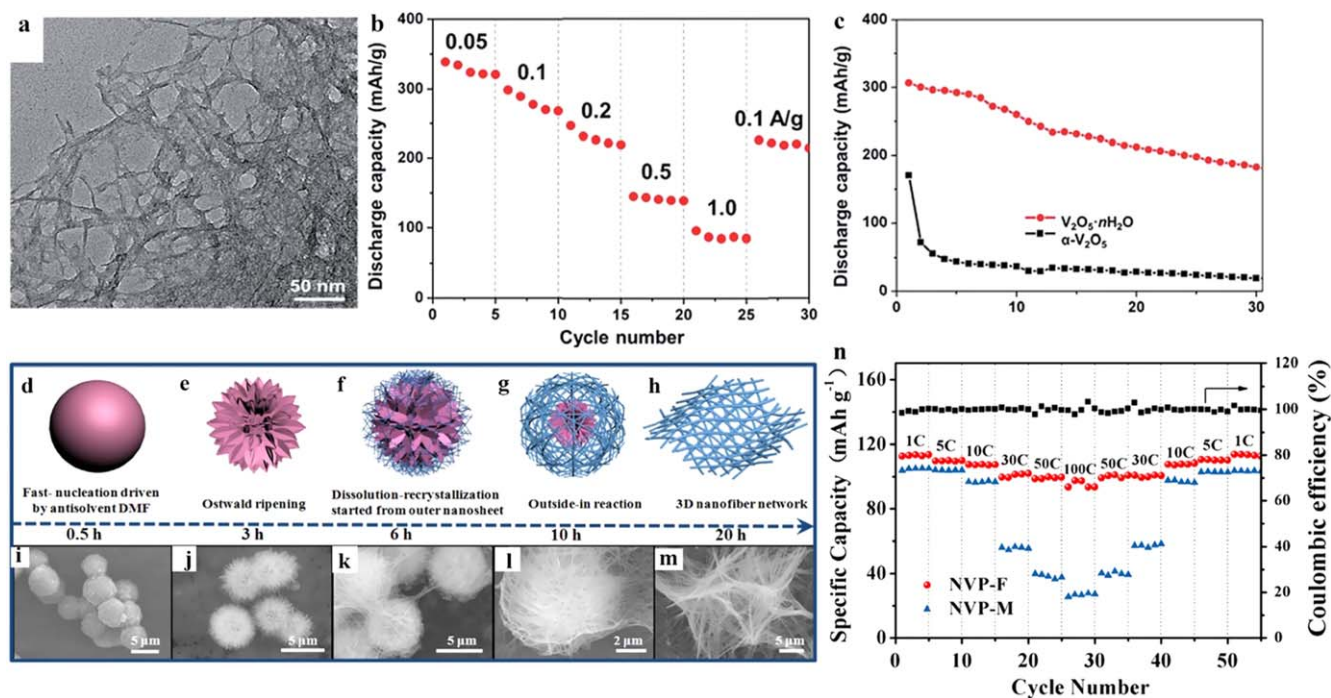
Figure 7. (a) A TEM image of the $V_2O_5 \cdot nH_2O$ xerogel. (b) The rate performance of the $V_2O_5 \cdot nH_2O$ cathode. (c) Cycling performance at the current density of 0.1 A g^{-1}. Reproduced from [20]. with permission of The Royal Society of Chemistry. (d-m) Schematic illustrations of the time-dependent solvothermal reaction: the self-sacrificed evolution mechanism from microsphere to nanofiber network. (n) Rate capability of the $Na_3V_2(PO_4)_3/C$ nanofiber network (NVP-F) and $Na_3V_2(PO_4)_3/C$ microflower (NVP-M) electrodes. Reprinted from [65]. Copyright 2016, with permission from Elsevier.

structures [62–64]. Herein, we will introduce several methods of synthesizing network/membrane structure electrode materials.

Recently, Wei *et al* synthesized a needle-like nanowire network $V_2O_5 \cdot nH_2O$ gel by a freeze-drying method [20], and the application of large-scale double-layer $V_2O_5 \cdot nH_2O$ to sodium storage in an organic electrolyte system was explored (figures 7(a)–(c)). They first thawed the V_2O_5 powder at 800 °C to form a melt. Next, the liquid was poured into distilled water during the stirring process to obtain a suspension. Then, the suspension was heated and cooled to obtain the sol, and then the sol was frozen to remove extra water. Finally, the sol was dried for 5 h in 120 °C air. The network structure $V_2O_5 \cdot nH_2O$ gel was used as a cathode for SIBs. It was found that an initial capacitance of 338 mA h g^{-1} at 0.05 A g^{-1} and a high rate capacity of 96 mA h g^{-1} at 1.0 A g^{-1} was obtained. However, the above method requires extremely high temperatures, and researchers are trying to find other simpler methods. For example, Ren *et al* [65] proposed a simple self-sacrificial template method to successfully fabricate a $Na_3V_2(PO_4)_3$ (NVP) 3D nanofiber network structure material to improve the electronic conductivity of the classical $Na_3V_2(PO_4)_3$ material, which obtained a good cycle stability (96.9% capacity retention over 300 cycles at 5 C) and excellent rate capacity (80 mA h g^{-1} at 50 C). The reaction was carried out under N, N-dimethylformamide antisolvent heat treatment. The NVP was rapidly nucleated and crystal growth occurred during the first 0.5 h of heat treatment to form a 3–5 micron microsphere. With an increase in the solvent heat treatment time to 3 h, the surface of the

microspheres gradually changed into the shape of the microflowers assembled by the nanosheets. Under the influence of the nucleophilic and electrophilic properties of the N-dimethylformamide, the surface nanosheets acted as self-sacrificing templates to dissolve and recrystallize to form nanofibers. Until the final solvent heat treatment for 20 h, the nanosheets disappeared completely, and a 3D network structure NVP was formed. The formation of 3D network structures provides faster transport channels for sodium ions, a larger contact area for the electrode–electrolyte, and possesses an excellent strain adaptability and structural integrity.

Meanwhile, another simple hydrothermal method has been proposed. Mai's group successfully synthesized flexible and additive-free $H_2V_3O_8$ nanowire films by a simple hydrothermal method [19]. They added deionized water and PEG to V_2O_5 to synthesize pure ultralong $H_2V_3O_8$ nanowires. Hyper acoustic treatment for an hour before filtration was carried out with a vinylidene fluoride membrane. Then, the membrane was removed and dried at room temperature for a few hours to remove the moisture contained within. Finally, $H_2V_3O_8$ thin films with a length of several hundred microns, a width of about 100 nanometers, and a thickness of about 35 microns were obtained. In a test of a SIB with $H_2V_3O_8$ nanowire film as the cathode, it was found that it showed a high sodium storage capacity (with a high specific capacity of 168 mA h g^{-1} at the current density of 10 mA g^{-1}). Chen *et al* synthesized a similar interpenetrating network structure composed of layered V_2O_5 nanowires and CNTs by a hydrothermal method [66]. The ultralong CNT arrays were synthesized by CVD and then dispersed in the V_2O_5 nanowire precursor (figure 8). Owing to the
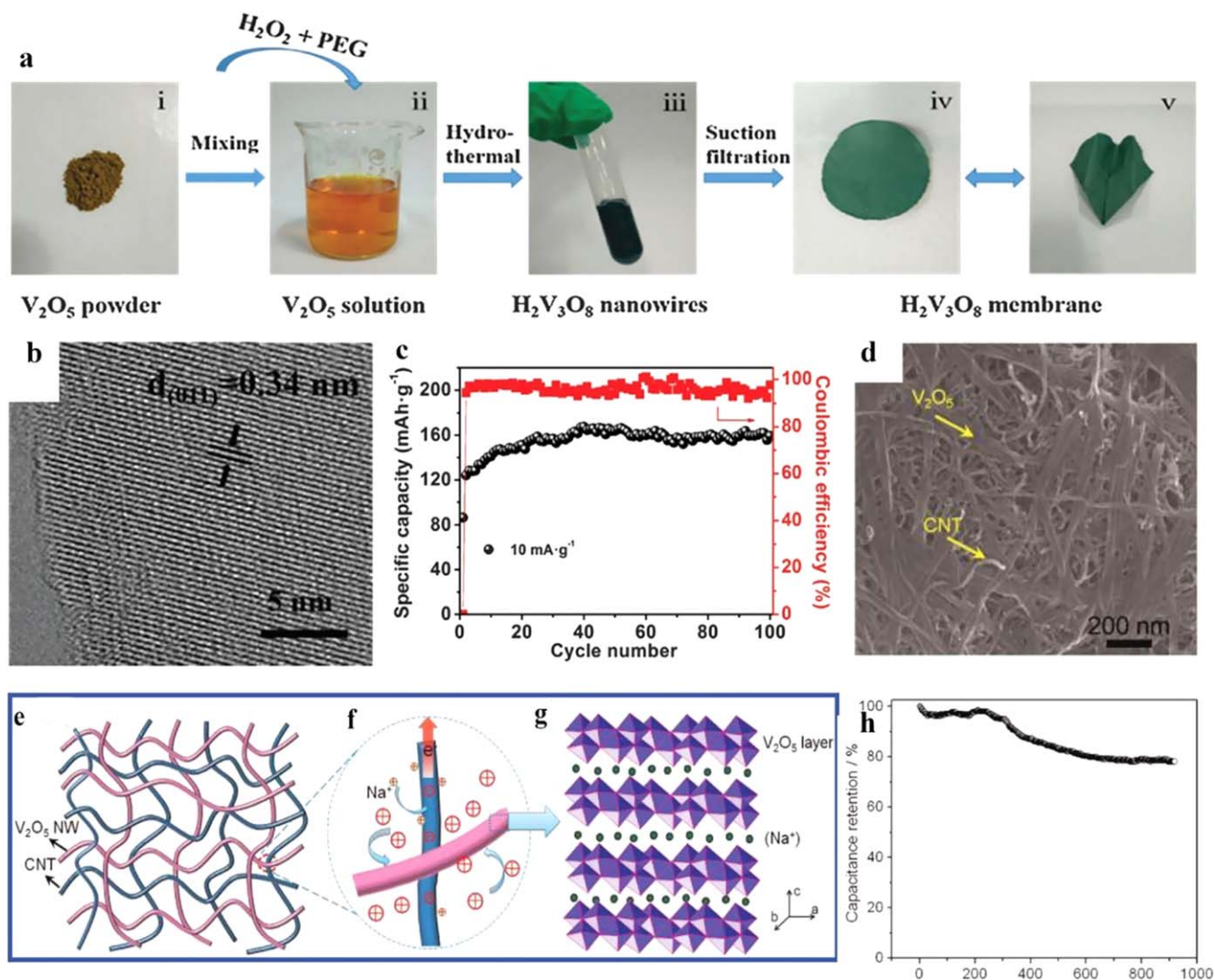
Figure 8. (a) A schematic illustration for the formation of the flexible additive-free $H_2V_3O_8$ nanowire membrane using a hydrothermal reaction followed by a suction filtration method. (b) HRTEM images of the $H_2V_3O_8$ nanowire membrane. (c) Cycling performance of the $H_2V_3O_8$ membrane at the current density of 10 mA g^{-1}. Reproduced from [19] with permission of The Royal Society of Chemistry. (d) A high-magnification SEM image of the nanocomposites etched by 1 wt% HF. The image corresponds to the selected area in panel B. A schematic of (e) a nanocomposite consisting of interpenetrating networks of V_2O_5 nanowires and CNTs, (f) intimate contacts between the V_2O_5 nanowire and CNTs facilitating charge transport, and (g) Na$^+$ intercalation within the V_2O_5 layer structure. (h) Cycling performance of a V_2O_5/CNT-AC sodium-ion device for 900 cycles at a charge/discharge rate of 60 C. Reprinted with permission from [66]. Copyright 2012 American Chemical Society.

strong interaction between −OH and −COOH on the surfaces of nanotubes and nanowires, the *in situ* hydrothermal reaction resulted in the formation of intermediates of the 3D nanostructures. Most importantly, the final composite network structure was obtained by filtration and concentration. The CNTs/V_2O_5 synthesized by this method had good electrochemical performance (80% of the initial capacity was retained after 900 cycles at a charge/discharge rate of 60 C), and it is proved that the sodium-ion asymmetric capacitor shows good energy and power density in organic electrolytes.

Tan *et al* put forward a new idea [14] in which they successfully prepared a $V_2O_3 \subset$ C-NTs $\subset$ rGO multi-dimensional cooperative nanowire structure, which solved the problem that 2D graphene and its 3D structure cannot limit the self-agglomeration of nanoparticles very well. The theory

of selective insertion and transformation of V_2O_3 in sodium-ion storage was also studied. To simplify the precursor of VO$_X$ nanotubes, VO$_X$-NTs were synthesized by cetylamine-assisted self-scrolling method. The precursor was dispersed in ethanol and graphene oxide nanoparticles were added to the ethanol. The cationic active agent CTAB was added to realize the self-assembly of VO$_X$-NTS $\subset$ GO by electrostatic action. After centrifugation, the VO$_X$-NTS $\subset$ GO was frozen rapidly in liquid nitrogen and annealed in a reducing atmosphere. The $V_2O_3 \subset$ C-NTs were embedded deeply in the rGO network and the structure was clearly observed by *in situ* electron microscopy. This special network structure leads to a good synergy between $V_2O_3 \subset$ C-NTs $\subset$ rGO (figure 9).

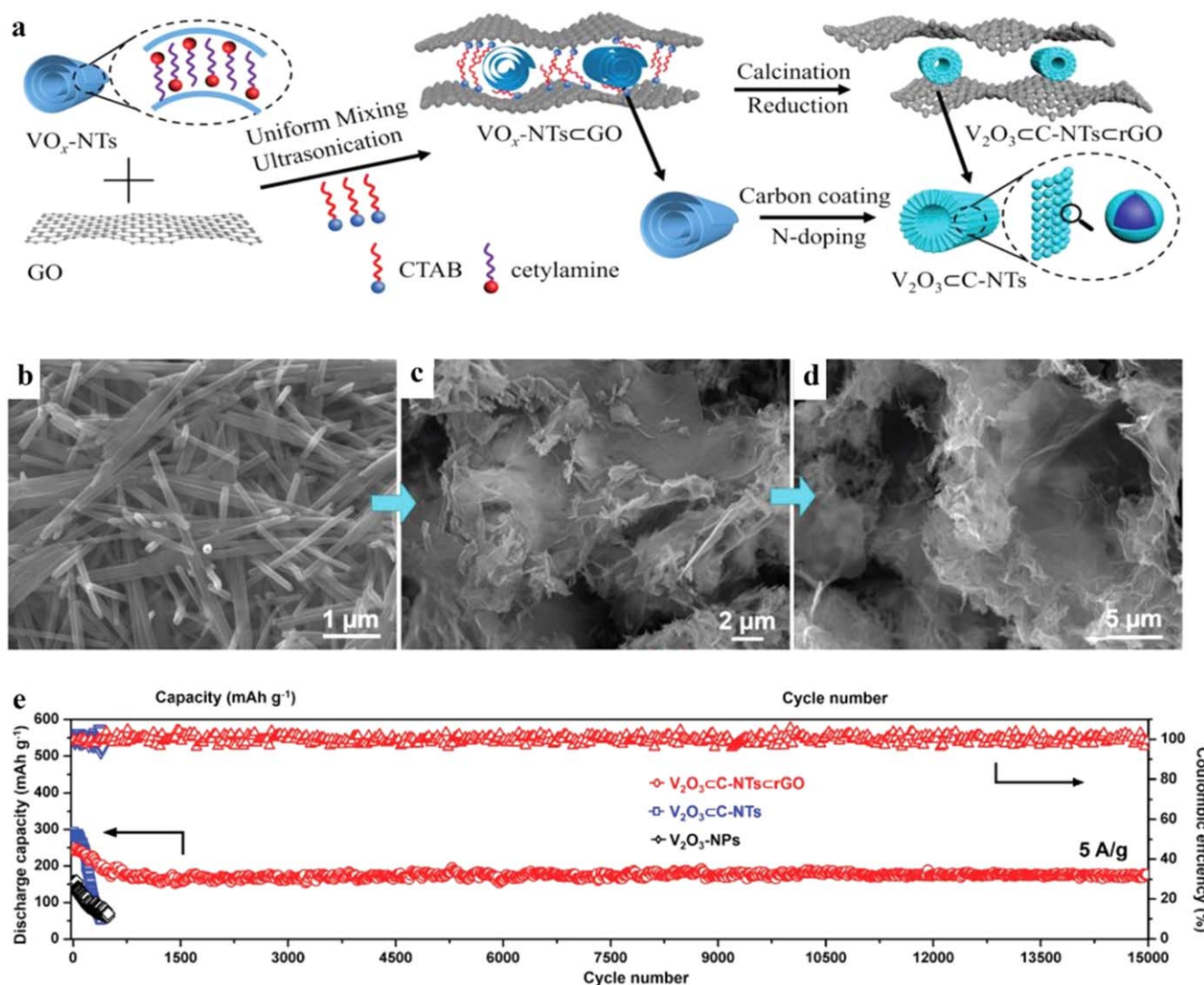In conclusion, the networked nanowire structures have stable layered skeleton structures, fast ion diffusion channels,

Figure 9. Synthesis and characterization of $V_2O_3 \subset C\text{-NTs} \subset rGO$. (a) A schematic of the synthesis of $V_2O_3 \subset C\text{-NTs} \subset rGO$. SEM images of (b) the VOx-NTs, (c) VOx-NTs $\subset$ GO, and (d) $V_2O_3 \subset C\text{-NTs} \subset rGO$. (e) Cycling performance and corresponding coulombic efficiency of $V_2O_3 \subset C\text{-NTs} \subset rGO$, $V_2O_3 \subset C\text{-NTs}$, and $V_2O_3\text{-NPs}$ at a high rate of 5.0 A g^{-1} (initially activated at 0.1 A g^{-1} for three cycles). [14] John Wiley & Sons. © 2018 WILEY-VCH Verlag GmbH & Co. KGaA, Weinheim.

and 3D electron transport networks, and have a strong potential for energy storage. This structure can be interpenetrating with the same nanowires, or intertwined with different nanowires, or even nanomaterials embedded in 3D nanowires. Network structures inherit most of the advantages of multiple nanowires, and researchers can also design different network structures to achieve the desired performance. Similarly, the membrane structures are usually more flexible, it is not easy to deform during charge and discharge, and the synthetic method is brief. Thus, the new 3D network structures or membrane structures can effectively improve the performance of the electrode.

3. Applications in SIBs

In recent years, the intelligent design and nanoarchitecture of LIB electrode materials with brilliant properties have been applied to the field of SIBs. However, SIBs suffer from issues of low power density like LIBs. It is therefore necessary to develop electrode materials with suitable voltage windows, high reversible capacity, and electrochemical stablity to improve the application of SIBs [8]. Vanadium-based materials possess high capacity, high energy density, and abundant resources, and therefore they are regarded as one of the most prospective electrode materials for advanced batteries. A large number of 1D vanadium-based materials have been fabricated and possess extremely high specificity, which aims to enhance the electrochemical properties of current materials [67]. In this section, promising cathode/anode materials will be briefly summarized, the effect of the material structure on battery performance will also be discussed, and the contribution of vanadium-based nanowire materials in SIB development will be highlighted to provide a new vision for SIBs. The key electrode materials are summarized in table 2 to provide a more intuitive understanding of the current status of SIBs.

Table 2. Key electrode materials for SIBs.

System	Materials	Specific capacity	Cycling stability	Working voltage (V)	Applications	Ref.
V-based nanowire materials	$Na_3V_2(PO_4)_3$ nanofiber network	94 mA h g^{-1} at 100 C	95.9% capacity retention over 1000 cycles at 10 C	2.3–3.9	Cathode	[65]
	Zigzag $Na_{1.25}V_3O_8$	172.5 mA h g^{-1} at 100 mA g^{-1}	Capacity fading 0.0138% per cycle at 1 A g^{-1} for 1000 cycles	1.5–4.0	Cathode	[6]
	$K_3V_2(PO_4)_3$/C	119 mA h g^{-1} at 100 mA g^{-1}	96.0% capacity retention after 2000 cycles at 2000 mA g^{-1}	1.5–4.0	Cathode	[4]
	CQD-coated VO_2	328 mA h g^{-1} at 0.3 C	70% capacity retention at 10 C After 200 cycles	1.5–3.5	Cathode	[49]
	$Cu_3V_2O_7(OH)_2 \cdot 2H_2O$	287.4 mA h g^{-1} at 0.5 A g^{-1}	206.5 mA h g^{-1} after 50 cycles at 5 A g^{-1}	0.01–3	Anode	[103]
	VO_2/rGO	160 mA h g^{-1} at 160 mA g^{-1}	200 mA h g^{-1} over 200 cycles	0.25–3	Anode	[107]
	CaV4O9	300 mA h g^{-1} at 5000 mA g^{-1}	161.5 mA h g^{-1} after 1000 cycles	0.01–3	Anode	[15]
Layered oxide materials	O_3-$Na[Li_{0.05}(Ni_{0.25}Fe_{0.25}Mn_{0.5})_{0.95}]O_2$	180.1 mA h g^{-1}g^{-1} at 0.1 C	76% capacity retention over 200 cycles	1.7–4.4	Cathode	[73]
	P_2-$Na_{2/3}[Mg_{0.28}Mn_{0.72}]O_2$	220 mA h g^{-1} at 10 mA g^{-1}	50% capacity retention after 200 cycles	1.5–4.4	Cathode	[72]
Polyanionic materials	$Na_3V_2(PO_4)_3$	66.3 mA h g^{-1} at 0.2 C	89% capacity retention after 200 cycles	1.0–3.0	Cathode	[68]
	$Na_4Co_3(PO4)_2P_2O_7$	95 mA h g^{-1} at 0.1 C	83% capacity retention after 100 cycles	3.0–4.7	Cathode	[69]
Prussian blue material	$FeFe(CN)_6$	120 mA h g^{-1} at 20 C	87% capacity retention over 500 cycles	2.0–3.8	Cathode	[70]
	$Na_2MnFe(CN)_6$	120 mA h g^{-1} at 20 C	75% capacity retention after 500 cycles at 0.7 C	0.01–3	Cathode	[71]
Carbon-based materials	Hollow carbon nanowires	250.9 mA h g^{-1} at 50 mA g^{-1}	82.2% capacity retention after 400 cycles	0.01–1.2	Anode	[91]
	3D porous carbon frameworks	113.9 mA h g^{-1} at 5 A g^{-1}	99.8 mA h g^{-1} after 10 000 cycles	0.01–3	Anode	[92]
Metal oxides	TiO_2/C	277.5 and 153.9 mA h g^{-1} at 50 and 5000 mA g^{-1},	100% capacity retention over 14,000 cycles at 5000 mA g^{-1}	0.01–3	Anode	[93]
	Co_3O_4	153.8 mA h g^{-1} at 5 A g^{-1}	1045.3 mA h g^{-1} after 100 cycles at 200 mA g^{-1}	0.005–2.9	Anode	[94]
Metal sulfides	Sb_2S_3	582 mA h g^{-1} at 200 mA g^{-1}	384 mA h g^{-1} at 200 mA g^{-1} after 50 cycles	0.01–2	Anode	[95]
Alloys	Sn-Sb	603 mA h g^{-1} at 100 mA g^{-1}	451.3 mA h g^{-1} at 500 mA g^{-1} after 150 cycles	0.01–2	Anode	[96]

3.1. Vanadium-based nanowire cathode in SIBs

Up to now, various cathode materials have been reported due to the rapid development of LIBs. With regards to SIB systems, four types of cathode materials have achieved meaningful advancement. Firstly, polyanionic cathode materials can provide excellent stability and rate capability, and are mainly phosphate-based compounds [68, 69]. Secondly, the Prussian blue analogue has many advantages, such as low cost and long cycle life, but it has an inferior specific capacity, which restricts mass production [70, 71]. And then, a series of P2-type layered transition metal oxides have been proposed in full-cell SIBs, which possess high rechargeable capacity and great cycling stability [72]. Nonetheless, the actual manufacture will be impeded because of the sodium deficiency of the P2-type layered cathode. Finally, O3-type layered transition metal compounds are considered as promising cathode materials because of their high energy density, high specific capacity, high initial coulombic efficiency, and good compatibility with anodes [73]. Most important of all, the preparative technique of SIB materials can be simply applied to industrial production. However, it is easy for them to deteriorate during storage [74].

Over the past few decades, vanadium-based materials have attracted considerable attention as promising cathode materials for batteries. However, there are some problems with these materials, such as unsatisfactory diffusion coefficients and structural degradation. Thus, increasing crystal structure stability and extending the ion diffusion channels of present cathode materials are the two main methods used for improving the material properties. Based on these principles, various important optimization strategies have been developed, including stable ion diffusion channels, crystal phase control, and ion doping, to achieve high-performance battery materials [75].

As a typical NA super ion conductor (NASICON)-based electrode material, $Na_3V_2(PO_4)_3$ (NVP) received wide attention because of the highly covalent 3D frameworks [76–78], which lead to high ionic conductivity and large interspaces. Song *et al* studied the ion occupancy change to explain the ion migration mechanism of $Na_3V_2(PO_4)_3$ at the first time. They found that two pathways along the x and y directions and one possible curved route for ion migration are beneficial for a 3D transport characteristic [79]. However, the phosphate components mean that NVP has low electronic conductivity [80, 81]. To address this situation, most researchers adopt the method of carbon coating. Shen *et al* fabricated a nitrogen-doped carbon-coated $Na_3V_2(PO_4)_3$ hybridized with multi-walled CNT composite. Nitrogen doping can improve the migration speed of Na ions through the carbon coating, and the 3D CNT network can significantly accelerate the electron transfer between multiple $Na_3V_2(PO_4)_3$ particles [82]. Similarly, $Na_3V_2(PO_4)_3$@C core–shell nanocomposites were synthesized by Duan *et al,* which delivered an initial capacity of 104.3 mA h g^{-1} at 0.5 C and 94.9 mA h g^{-1} at 5 C with a capacity retention of 96.1% after 700 cycles [83]. Other methods such as changing the configuration of materials have

also been proven to successfully solve this issue. Ren *et al* first put forward a facile self-sacrificed route to synthesize a 3D NVP nanofiber network [65]; after a time-dependent experiment, a continuous outside-in 3D network was raised. The 3D electrochemical and mechanical properties of the NVP network structure material enhanced the high current performance, which exhibited outstanding cycle stability (95.9% capacity retention over 1000 cycles at 10 C) and high rate performance (94 mA h g^{-1} at 100 C). Liu reported a 1D nanostructure material using $Na_3V_2(PO_4)_3$ as the cathode material [23], which shows superior cycling stability, even at high current rates, because of its short ion diffusion length and suitable access of the organic electrolyte. In addition, compared to premier preparation through solid-state and solution reactions, a simple versatile electrospinning method to fabricate a $Na_3V_2(PO_4)_3$/carbon nanofiber electrode was reported [23], and this method handled the traditional problem of poor performance far away from the theoretical capacity. However, this structure shows defects compared with the $Na_3V_2(PO_4)_3$ porous nanoparticle; its rate capability is lower, which may relate to its long annealing treatment and high content of carbon.

With regards to traditional electrode materials, including polymeric binders, conductive additives, and current collectors, the conductive additives and current collectors can be used to ensure material mechanical performance security and increase the electrical contact between active materials and current collectors. However, the existence of the polymer will hinder the electrical conductivity, occupying about 20%–40% of the electrode material's quality [84, 85]. In addition, the active material can easily fall off the conductive metal foil. Wang *et al* synthesized a novel additive-free electrode composed of an ultralong $H_2V_3O_8$ nanowire membrane (figures 10(a)–(c)) [19], which provided a steady structure and high specific capacity. Dong *et al* synthesized hierarchical zigzag structured $Na_{1.25}V_3O_8$ nanowires via a facile topotactic intercalation method (figures 10(d)–(h)) [6]. The material obtained good electrochemical performance. This specific structure has better adaptability strain and promotes the contact area between the electrode and the integrity and stability of the structure. Wang *et al* designed a novel $K_3V_2(PO_4)_3$/C bundled nanowire structure by using a facile organic acid-assisted method to improve the poor cycling stability and low diffusion coefficient [4]. With the nanoporous structure, the battery shows excellent electrochemical performance. Besides changing the structure of the electrode material, metal-doped materials are also a concept for improving the performance. Mai's group doped alkali metal ions (Li^+, Na^+, K^+, Rb^+) into vanadium oxide nanowires [86]. After the electrochemical test, it was found that the appropriate alkali metal-ion intercalation in the admissible layered structure can avoid structure collapse, resulting in enhanced cycling stability [11]. Furthermore, carbon material doping is also a valuable method. Balogun *et al* designed a new type of free-standing CQD-coated VO_2 interwoven nanowire through a simple fabrication process [49]. CQDs
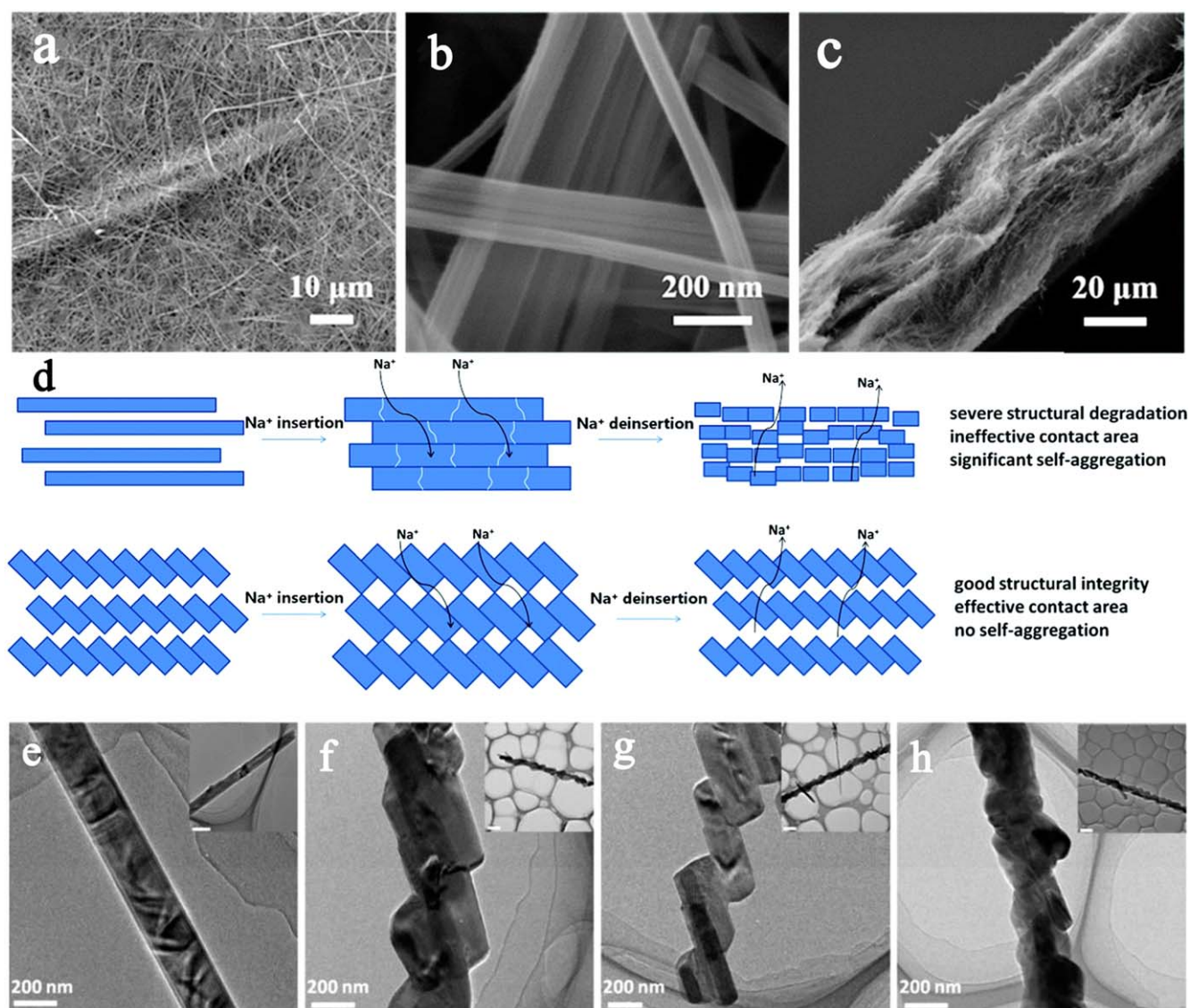
Figure 10. Front (a) and (b) and side (c) SEM images of the $H_2V_3O_8$ nanowire membrane. Reproduced from [19] with permission of The Royal Society of Chemistry. (d) A schematic illustration of the electrochemical process for the non-topotactically synthesized simple nanowire structure and topotactically synthesized hierarchical zigzag nanowire structure of $Na_{1.25}V_3O_8$. (e)–(i) Morphologies of products synthesized with different amounts of CTAB. (e) TEM images of simple NVO, (f) NVO-C1, (g) NVO-C2, and (h) NVO-C3. Reproduced from [6] with permission of The Royal Society of Chemistry.

can effectively protect the surface of the nanowires due to good flexibility, which makes a great contribution to the diffusion of the electrons. Carbon materials coat the internal and external surfaces of the VO_2 nanowires, and this unique structure effectively improves the capacity of the electrode materials. Chen *et al* designed an interpenetrating porous network structure material which was composed of CNTs and V_2O_5 nanowires [66]. This structure makes electron transfer easily, improves the kinetics and cycle stability, and enables the fabrication of high-performance Na-ion pseudocapacitors. Mallory *et al* studied the structural changes in sodium pre-intercalated vanadium oxides [28]. The pre-intercalation for the specific structure of the electrode material is a crucial synthetic method. With the carrier of the V_2O_5 embedded with a number of Na ions, a highly crystalline nanowire structure was obtained with the specific capacity of 365 mA h g^{-1}. The work

shows that improvement in the structure of electrode materials and suitable materials with certain metal elements can fundamentally increase the properties of the material. It has a great potential to develop the energy density of the electrode materials and power density. as well as internal ion diffusion. The Yu group developed an effective interlayer engineering strategy to improve sodium-ion transport in 2D $VOPO_4$ nanosheets via controlled organic intercalation. The interlayer distance of $VOPO_4$ nanosheets can be easily adjusted by embedding organic molecules with different interlayer distances. The $VOPO_4$ nanosheets showed improved sodium-ion transport kinetics, remarkable rate capacity, and cycling stability of sodium-ion storage [87]. A sodium-ion full battery based on this cathode has also been fabricated, showing outstanding rate capability ($\sim$74 mA h g^{-1} at 2 C rate) and excellent cycling stability (92.4% capacity retention after 100 cycles) [88].

3.2. Vanadium-based nanowire anode in SIBs

To acquire the valuable characteristics of LIBs, a considerable amount of effort has been made in SIBs, and some lithium-ion intercalation materials with typical layered materials can also be used for SIBs. A larger ionic radius (Na^+ 0.102 nm, Li^+ 0.076 nm) leads to slow reaction kinetics, often leading to reduced capacity, poor rate capability, poor cycle stability, and even no electrochemical activity. After years of hard work, significant progress has also been made in cathode materials for SIBs [74]. However, the limited electrochemical properties of anode materials significantly influence the progression of SIBs. In the case of graphite, it is the most commonly used anode material in LIBs. However, due to the limited insertion of sodium-ions into graphite, graphite is not an ideal anode for SIBs, and calculations show that the higher formation energy of graphite and sodium ions leads to thermodynamic instability, which greatly hinders the sodium–graphite reaction [89]. By using an ether solvent (DEGDME), a complex will be formed between the sodium-ion and the ether group to change the affinity of the Na–C bond via a co-intercalation reaction [90].

Hard carbon is probably the most widely studied anode material of SIBs, because the hard carbon layer spacing is large, which facilitates the storage of Na^+. However, the initial coulombic efficiency and cycle life issues are still unsatisfactory. The manufacture of hollow carbon nanowires and hollow carbon nanospheres provides new ideas for the development of carbon materials [91, 92]. The unique shape can effectively explain that sodium is bound to the thin layer of carbon, which also relaxes the volume expansion during the deintercalation process while locking the sodium.

Other anode materials (e.g. TiO_2, Co_3O_4, and Sb_2S_3) based on the conversion or alloying reaction can provide high initial capacity, but large volume changes that are unavoidable during the cycle result in pulverization of the electrode and subsequent severe capacity decay [93–96]. Vanadium has multiple valence states, and it can achieve electron transfer at a low potential. Moreover, the high V–O bonding strength determines that vanadium cannot be reduced to metallic V at low potential, which means a smaller volume expansion during the cycle. The above advantages provide the vanadium material with a high capacity and cycling stability [15, 97].

A novel a-$CrPO_4$-type $NaV_3(PO_4)_3$ was synthesized by Wang *et al* as a promising anode material for SIBs. They also studied the electrochemical reaction mechanism, structural evolution, and ion diffusion of $NaV_3(PO_4)_3$ by first-principles calculation. These works are of great significance and provide guidance to understand the 3D characteristics for ion transport by exploration of the internal diffusion systems [98]. Deng *et al* designed a novel 1D nanostructure material for aqueous SIBs [99]. As an important department of vanadium oxide, $Na_2V_6O_{16} \cdot nH_2O$ shows a typical lamellar structure, with sodium hydrate existing in the V_3O_8 layer. It provides enough layer spacing for the Na^+ intercalation. Furthermore, the atomically anisotropic arrangement in the crystal lattice results in an infinite chain structure, which has the potential to grow into a 1D nanostructure with a unique direction [100, 101]. Due to this higher 1D nanostructure's current transmission efficiency, it can improve teh performance of the electrode materials. Since the radius of the sodium ion is larger than that of lithium, there are many issues with finding a suitable electrode material to allow reversible, rapid Na-ion insertion and extraction at high rates [102, 103]. To solve this problem, Liang *et al* synthesized intertwined $Cu_3V_2O_7(OH)_2 \cdot 2H_2O$ nanowire/carbon fiber composite as an anode material [104], which offered a wider potential window. Vanadium-based materials with sufficient layer spacing are greatly beneficial for Na^+ insertion/extraction. In addition, the 1D nanowire structure provides assistance for reducing the Na-ion diffusion length. Meanwhile, numerous interconnected pore channels created by the intertwined network facilitate the access of electrolytes and electrode, thereby improving the accessibility of the cell at high rates [105, 106]. This material has good electrochemical performance, showing a highly reversible Na-ion storage capacity of 287.4 mA h g^{-1} after 50 cycles at a large current density of 0.5 A g^{-1}. For easier preparation of VO_2, He *et al* developed a solution-based strategy to prepare VO_2 by reducing aqueous vanadate ions in KOH medium [107], which was applied in LIBs and SIBs with good electrochemical performance and cycle performance. Even under low voltage, the anode materials maintained high cycle performance and structure stability. Short ion diffusion pathways and effective electron transport capability are considered to be some of the most ideal properties for the application of the energy storage system architecture, especially for 1D nanostructure material directional arrangement [108]. Ke *et al* designed and constructed an aligned $NaV_3(PO_4)_3/C$ hybrid nanofiber as an anode in SIBs with a steady skeleton, resulting in an excellent long cycle and high rate performance, which makes it a promising anode for SIBs [109]. Xu *et al* fabricated CaV_4O_9 nanowires with a specific Na^+ storage mechanism beyond the typical intercalation or conversion reaction and which exhibited multiple positive electrochemical properties [15]. The nanoscale CaO can lead to a 'spectator effect' to restrain the volume change in the electrode and can inhibit the aggregation of active nanoparticles. Compared with the cathode materials, the amount of vanadium-based anode material in sodium electricity is rare, and the capacity makes it difficult to meet the requirements. More attention should be placed on the anode materials to create new high-performance materials.

3.3. Single-nanowire devices used in SIBs

A large number of materials have been fabricated and improved for energy storage, and the complex reaction mechanisms are still the bottleneck of development. Although some studies have reported the properties of numerous nanomaterials, most of the research is based on the macroscopic properties of nanowire powders, which will be affected by grain boundaries and material disorder, and therefore cannot truly reflect the intrinsic properties of the materials. The construction of single-nanowire devices is more likely to
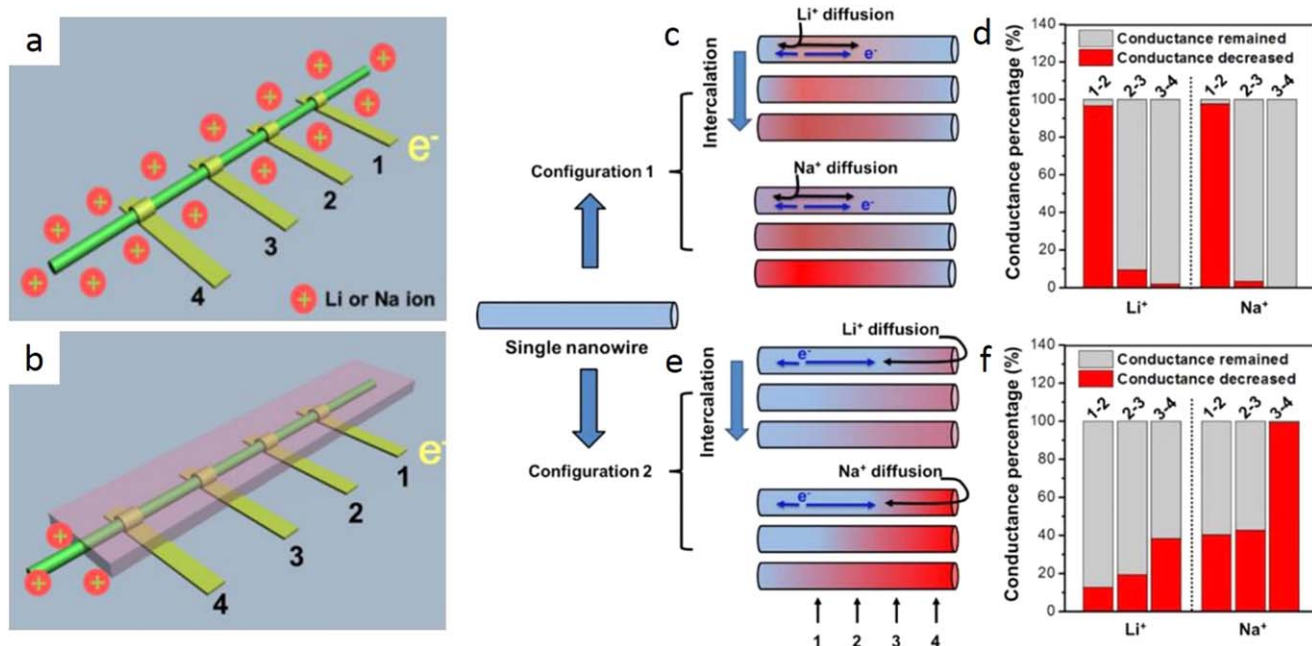
Figure 11. The contact of nanowire and Au (1, 2, 3 and 4) is used for electric and electrochemical tests. (a) Configuration 1: the $H_2V_3O_8$ nanowire was fully immersed in the electrolyte. (b) Configuration 2: only one end of the $H_2V_3O_8$ nanowire was immersed in the electrolyte and the other area was covered by the photoresist. (c) A schematic illustration of the diffusion for Li/Na ions and (d) their conductance changes in configuration 1. (e) A schematic illustration of the diffusion for Li/Na ions and (f) their conductance changes in configuration 2. Reprinted with permission from [114]. Copyright 2015 American Chemical Society.

directly reflect the intrinsic mechanism of materials in electrochemical processes [110].

Since nanowires are usually micrometer-scale in length and nanometer-scale in diameter, the conductivity of electrons and intercalation/deintercalation of ions along these 1D materials tremendously influences their electrochemical performance in Li^+/Na^+ batteries. On account of this, our group fabricated single-nanowire devices to detect their degradation mechanism during electrochemical reactions [32, 111–114]. In our works, the single nanowires were connected with the Au current collector by lithography-based techniques in different configurations, and electrochemical tests were conducted *in situ* to investigate the mechanism relevant to the migration of ions and degradation of electrochemical performance.

To thoroughly investigate the transport properties of Na^+ in nanoscale electrodes, Xu *et al* fabricated two types of single-nanowire devices (figures 11(a), (b)) [114]. In both configurations, four contacts were designed. Contact 1 was employed to conduct the electrochemical tests and the others were used to test the electric conductivity. In configuration 1, the $H_2V_3O_8$ nanowire was exposed to the electrolyte, whereas in configuration 2, only one end was exposed to the electrolyte and the other area was covered by a photoresist. The electric conductivity of sections 1–4 in configurations 1 and 2 were tested respectively. For configuration 1, the sections with the shorter distance from contact 1 exhibited more severe degradation in electric conductivity, which indicates that the longer distance made the electron transport more difficult and intercalation of Na^+ chose the shortest pathway (figures 11(c), (d)). For configuration 2, the electric

conductivity decreases more sharply with the longer distance from contact 1, indicating that the electrochemical reaction can only be realized when the electrons and ions are both accessible (figures 11(e), (f)). This research was significant in that it revealed the transport mechanism of Na^+ in the nanoelectrode and will pave the way for choosing suitable electrode materials for Na^+ batteries.

4. Conclusion and perspectives

This review has reported diverse nanostructures of vanadium-based nanowires and has highlighted the significance of constructing various nanostructures to obtain excellent electrochemical performance. Firstly, four popular nanowire-based nanostructures and various synthetic methods have been introduced. Configuring adequate pore size can deliver more reactive sites and shorten the Na^+ diffusion pathway. Considering the intrinsic poor electronic conductivity of electrode materials, core–shell structures coated with appropriate materials can enhance the electronic transmission and also alleviate the volume expansion of electrode materials during charge and discharge. Nanowire arrays and networks/membranes construct a stable 3D framework to provide multiple reaction areas and more spare room to buffer the volume change. Other heterostructure materials combine the advantages of different materials to build a more stable system. Secondly, the application of vanadium-based nanowires in the cathode and anode of SIBs has been summarized. With regards to the cathode, vanadium-based phosphate materials (NASICON) play an important role in the application of SIBs.

However, the exposed problem of low capacity also urgently needs to be solved. In terms of vanadium-based anode materials, the application is far behind that of the cathode. According to the contrast between current mainstream materials, we can find both the breakthroughs and challenges of vanadium-based materials. In particular, a single-nanowire device based on vanadium-based nanowires has been introduced, which excludes the influence of grain boundaries and disordering of materials, providing a direct approach to explore the capacity decay mechanism of materials in depth. Single-nanowire devices can make more contributions to the intrinsic properties research of nanowire materials.

Although researchers have made great efforts to accelerate the development of SIBs, they are still far from expectations. On the one hand, for the current materials, they should be widely extended to improve electrochemical performance and increase application. The unique structures of nanowire materials need to be created to meet the urgent demands of improvement, and many nanowire structures with great progress in LIBs have not been used in SIBs. For example, pre-embedding of materials can help solve the problem of low initial coulombic efficiency and poor cycle stability [86]. Coating MnO_2 nanowires with porous graphene can improve the conductivity of materials without hindering ion conduction [111]. The new pea-like nanotubes synthesized by a gradient electrospinning and controlled pyrolysis method exhibit superior cycling stability [115]. In addition, there is an urgent demand to further develop new high-efficiency sodium storage materials, such as CaV_4O_9. On the other hand, it is necessary to strengthen the understanding of the Na^+ storage mechanism, theoretically guiding the improvement of SIBs. Although Na^+ shares a similar storage mechanism with Li^+, most of the traditional materials used in LIBs still do not work well in SIBs. Therefore, the application of mechanism research, such as the application of a single-nanowire device, will play a key role in the progress of energy storage. Last but not least, for vanadium-based nanowires, they can be used in more fields due to their sufficient length and strength. The free-standing nanowire networks/membranes described above are expected to perform well in flexible batteries, and can be used in combination with solid electrolytes and many other devices.

We hope that SIBs can stand at the forefront of the energy storage era as soon as possible. There are more scientific methods to improve the properties of current materials, novel high-efficiency materials to improve the overall performance of SIBs, and more advanced technology to explore the mechanism of sodium-ion storage. Furthermore, vanadium-based nanowire materials can be used in more fields with better properties.

Contributions

L X and L M proposed the topic of the manuscript. C Y, Y X, Y C, and Q L wrote the manuscript. L X, L M, C Y, Y X, Y C, Q L, and T G discussed and revised the manuscript.

Conflict of interest

The authors declare no conflict of financial interest.

ORCID iDs

Liqiang Mai ⓘ https://orcid.org/0000-0003-4259-7725

Reference

[1] Li H S, Peng L L, Zhu Y, Zhang X G and Yu G H 2016 *Nano Lett.* **16** 5938–43
[2] Wei Q L, Xiong F Y, Tan S S, Huang L, Lan E H, Dunn B and Mai L Q 2017 *Adv. Mater.* **29** 1602300
[3] Mai L Q, Xu X, Xu L, Han C H and Luo Y Z 2011 *J. Mater. Res.* **26** 2175–85
[4] Wang X P *et al* 2015 *Adv. Energy Mater.* **5** 1500716
[5] Luo W, Calas A, Tang C J, Li F, Zhou L and Mai L Q 2016 *ACS Appl. Mater. Inter.* **8** 35219–26
[6] Dong Y F *et al* 2015 *Energy Environ. Sci.* **8** 1267–75
[7] Hartung S, Bucher N, Nair V S, Ling C Y, Wang Y, Hoster H E and Srinivasan M 2014 *Chemphyschem* **15** 2121–8
[8] Wang Q H, Xu J T, Zhang W C, Mao M L, Wei Z X, Wang L, Cui C Y, Zhu Y X and Ma J M 2018 *J. Mater. Chem.* A **6** 8815–38
[9] Mai L Q, Tian X C, Xu X, Chang L and Xu L 2014 *Chem. Rev.* **114** 11828–62
[10] Yu K S, Pan X L, Zhang G B, Liao X B, Zhou X B, Yan M Y, Xu L and Mai L Q 2018 *Adv. Energy Mater.* **8** 1802369
[11] Mai L Q, Sheng J Z, Xu L, Tan S S and Meng J S 2018 *Acc. Chem. Res.* **51** 950–9
[12] Xu Z L, Park J, Yoon G, Kim H and Kang K 2018 *Small Methods* 1800227
[13] Su D W and Wang G X 2013 *Acs Nano* **7** 11218–26
[14] Tan S S *et al* 2018 *Adv. Mater.* **30** 1707122
[15] Xu X M *et al* 2017 *Nat. Commun.* **8** 460
[16] Xu Y N, Wei Q L, Xu C, Li Q D, An Q Y, Zhang P F, Sheng J Z, Zhou L and Mai L Q 2016 *Adv. Energy Mater.* **6** 1600389
[17] Hu P *et al* 2018 *Nano Lett.* **18** 1758–63
[18] Tang H, Xu N, Pei C Y, Xiong F Y, Tan S S, Luo W, An Q Y and Mai L Q 2017 *ACS Appl. Mater. Inter.* **9** 28667–73

[19] Wang D, Wei Q L, Sheng J Z, Hu P, Yan M Y, Sun R M, Xu X M, An Q Y and Mai L Q 2016 *Phys. Chem. Chem. Phys.* **18** 12074–9

[20] Wei Q L, Liu J, Feng W, Sheng J Z, Tian X C, He L, An Q Y and Mai L Q 2015 *J. Mater. Chem.* A **3** 8070–5

[21] Sun R M, Wei Q L, Li Q D, Luo W, An Q Y, Sheng J Z, Wang D, Chen W and Mai L Q 2015 *Acs Appl. Mater. Interfaces* **7** 20902–8

[22] Yang C H, Ou X, Xiong X H, Zheng F H, Hu R Z, Chen Y, Liu M L and Huang K 2017 *Energy Environ. Sci.* **10** 107–13

[23] Liu J, Tang K, Song K P, van Aken P A, Yu Y and Maier J 2014 *Nanoscale* **6** 5081–6

[24] Devan R S, Patil R A, Lin J H and Ma Y R 2012 *Adv. Funct. Mater.* **22** 3326–70

[25] Aricò A S, Bruce P, Scrosati B, Tarascon J M and Van Schalkwijk W 2005 *Nat. Mater.* **4** 366–77

[26] Gao M R, Xu Y F, Jiang J and Yu S H 2013 *Chem. Soc. Rev.* **42** 2986–3017

[27] Lee Y, Oh S M, Park B, Ye B U, Lee N S, Baik J M, Hwang S J and Kim M H 2017 *Crystengcomm* **19** 5028–37

[28] Clites M, Byles B W and Pomerantseva E 2016 *J. Mater. Chem.* A **4** 7754–61

[29] Jiang Y, Yao Y, Shi J N, Zeng L C, Gu L and Yu Y 2016 *Chemnanomat.* **2** 726–31

[30] He P, Quan Y L, Xu X, Yan M Y, Yang W, An Q Y, He L and Mai L Q 2017 *Small* **13** 1702551

[31] An Q Y, Sheng J Z, Xu X, Wei Q L, Zhu Y Q, Han C H, Niu C J and Mai L Q 2014 *New J. Chem.* **38** 2075–80

[32] Mai L Q, Dong Y J, Xu L and Han C H 2010 *Nano Lett.* **10** 4273–8

[33] Xiong C, Aliev A E, Gnade B and Jr B K 2008 *Acs Nano* **2** 293–301

[34] Mai L Q, Xu L, Han C H, Xu X, Luo Y Z, Zhao S Y and Zhao Y L 2010 *Nano Lett.* **10** 4750–5

[35] Peng X Y, Yang Y M, Hou Y S, Travaglini H C, Hellwig L, Hihath S, van Benthem K, Lee K, Liu W F and Yu D 2016 *Phys. Rev. Appl.* **5** 054008

[36] Lee J, Kim J and Hyeon T 2006 *Adv. Mater.* **18** 2073–94

[37] Zhang L, Zhao K N, Xu W W, Meng J S, He L, An Q Y, Xu X, Luo Y Z, Zhao T W and Mai L Q 2014 *RSC Adv.* **4** 33332–7

[38] An Q Y, Zhang P F, Wei Q L, He L, Xiong F Y, Sheng J Z, Wang Q Q and Mai L Q 2014 *J. Mater. Chem.* A **2** 3297–302

[39] Lu X H, Yu M H, Zhai T, Wang G M, Xie S L, Liu T Y, Liang C L, Tong Y X and Li Y 2013 *Nano Lett.* **13** 2628–33

[40] Xiao X, Peng X, Jin H Y, Li T Q, Zhang C C, Gao B, Hu B, Huo K F and Zhou J 2013 *Adv. Mater.* **25** 5091–7

[41] Li Z T, Liu G X, Guo M, Ding L X, Wang S Q and Wang H H 2015 *Electrochim. Acta* **173** 131–8

[42] An G H, Lee D Y and Ahn H J 2016 *ACS Appl. Mater. Inter.* **8** 19466–74

[43] Yang G L, Ding B, Wang J, Nie P, Dou H and Zhang X G 2016 *Nanoscale* **8** 8495–9

[44] Wang L J, Zhang K, Hu Z, Duan W C, Cheng F Y and Chen J 2014 *Nano Res.* **7** 199–208

[45] Oh S, Lee J K, Byun D, Cho W I and Won Cho B 2004 *J. Power Sources* **132** 249–55

[46] Yan M Y *et al* 2013 *J. Am. Chem. Soc.* **135** 18176–82

[47] Mai L Q, Dong F, Xu X, Luo Y Z, An Q Y, Zhao Y L, Pan J and Yang J N 2013 *Nano Lett.* **13** 740–5

[48] Peng M H, Li B, Yan H J, Zhang D T, Wang X Y, Xia D G and Guo G S 2015 *Angew. Chem. Int. Ed.* **54** 6452–6

[49] Balogun M S, Luo Y, Lyu F Y, Wang F X, Yang H, Li H B, Liang C L, Huang M, Huang Y C and Tong Y X 2016 *ACS Appl. Mater. Inter.* **8** 9733–44

[50] Mai L Q, Xu X, Han C H, Luo Y Z, Xu L, Wu Y A and Zhao Y L 2011 *Nano Lett.* **11** 4992–6

[51] Khan Z, Senthilkumar B, Park S O, Park S, Yang J, Lee J H, Song H-K, Kim Y, Kwak S K and Ko H 2017 *J. Mater. Chem.* A **5** 2037–44

[52] Wang K, Wu H P, Meng Y N and Wei Z X 2014 *Small* **10** 14–31

[53] Wang K, Zhao P, Zhou X M, Wu H P and Wei Z X 2011 *J. Mater. Chem.* **21** 16373

[54] Xu J, Wang K, Zu S Z, Han B H and Wei Z X 2010 *Acs Nano* **4** 5019

[55] Chao D L *et al* 2015 *Nano Lett.* **15** 565–73

[56] Chao D L *et al* 2018 *Adv. Energy Mater.* **8** 1800058

[57] Liao J Y and Manthiram A 2015 *Nano Energy* **18** 20–7

[58] Wang H K, Gao X P, Feng J K and Xiong S L 2015 *Electrochim. Acta* **182** 769–74

[59] Xia X H, Chao D L, Zhang Y Q, Zhan J Y, Zhong Y, Wang X L, Wang Y D, Shen Z X, Tu J P and Fan H J 2016 *Small* **12** 3048–58

[60] Long J W, Dunn B, Rolison D R and White H S 2004 *Chem. Rev.* **35** 4463–92

[61] Zhang J, Guo L, Meng Q Y, Wang W Q, Liu M H, Jin Z and Zhao K 2018 *J. Mater. Sci.* **53** 13156–72

[62] Fu K *et al* 2017 *Energy Environ. Sci.* **10** 1568–75

[63] Gnana Kumar G, Chung S H, Raj Kumar T and Manthiram A 2018 *ACS Appl. Mater. Inter.* **10** 20627–34

[64] Talin A A, Ruzmetov D, Kolmakov A, McKelvey K, Ware N, El Gabaly F, Dunn B and White H S 2016 *ACS Appl. Mater. Inter.* **8** 32385–91

[65] Ren W H, Zheng Z P, Xu C, Niu C J, Wei Q L, An Q Y, Zhao K N, Yan M Y, Qin M S and Mai L Q 2016 *Nano Energy* **25** 145–53

[66] Chen Z, Augustyn V, Jia X L, Xiao Q F, Dunn B and Lu Y F 2012 *Acs Nano* **6** 4319–27

[67] Liu P C, Zhu K J, Gao Y F, Luo H J and Lu L 2017 *Adv. Energy Mater.* **7** 1700547

[68] Jian Z L, Zhao L, Pan H L, Hu Y S, Li H, Chen W and Chen L Q 2012 *Electrochem. Commun.* **14** 86–9

[69] Nose M, Nakayama H, Nobuhara K, Yamaguchi H, Nakanishi S and Iba H 2013 *J. Power Sources* **234** 175–9

[70] Lu Y H, Wang L, Cheng J H and Goodenough J B 2012 *Chem. Commun.* **48** 6544–6

[71] Song J, Wang L, Lu Y H, Liu J, Guo B K, Xiao P H, Lee J J, Yang X Q, Henkelman G and Goodenough J B 2015 *J. Am. Chem. Soc.* **137** 2658–64

[72] Yabuuchi N, Hara R, Kubota K, Paulsen J, Kumakura S and Komaba S 2014 *J. Mater. Chem.* A **2** 16851–5

[73] Oh S M, Myung S T, Hwang J Y, Scrosati B, Amine K and Sun Y K 2014 *Chem. Mater.* **26** 6165–71

[74] Deng J Q, Luo W B, Chou S L, Liu H K and Dou S X 2018 *Adv. Energy Mater.* **8** 1701428

[75] Meng J S, Guo H C, Niu C J, Zhao Y L, Xu L, Li Q and Mai L Q 2017 *Joule* **1** 522–47

[76] Zhu C B, Song K P, van Aken P A, Maier J and Yu Y 2014 *Nano Lett.* **14** 2175–80

[77] Chotard J-N, Rousse G, David R, Mentré O, Courty M and Masquelier C 2015 *Chem. Mater.* **27** 5982–7

[78] Zhang W, Liu Y T, Chen C J, Li Z, Huang Y H and Hu X L 2015 *Small* **11** 3822–9

[79] Song W X, Ji X B, Wu Z P, Zhu Y R, Yang Y C, Chen J, Jing M J, Li F Q and Banks C E 2014 *J. Mater. Chem.* A **2** 5358–62

[80] An Q Y, Xiong F Y, Wei Q L, Sheng J Z, He L, Ma D L, Yao Y and Mai L Q 2015 *Adv. Energy Mater.* **5** 1401963

[81] Li S, Dong Y F, Xu L, Xu X, He L and Mai L Q 2014 *Adv. Mater.* **26** 3545–53

[82] Shen W, Li H, Guo Z Y, Wang C, Li Z H, Xu Q J, Liu H M, Wang Y G and Xia Y Y 2016 *ACS Appl. Mater. Inter.* **8** 15341–51

[83] Duan W C, Zhu Z Q, Li H, Hu Z, Zhang K, Cheng F Y and Chen J 2014 *J. Mater. Chem.* A **2** 8668–75

[84] Hu L b, Choi J W, Yang Y, Jeong S, La M F, Cui L F and Cui Y 2009 *Proc. Natl. Acad. Sci. USA* **106** 21490–4

[85] Cui L F, Hu L, Choi J W and Cui Y 2010 *Acs Nano* **4** 3671–8

[86] Zhao Y L *et al* 2015 *Nano Lett.* **15** 2180–5

[87] Peng L L, Zhu Y, Peng X, Fang Z W, Chu W S, Wang Y, Xie Y J, Li Y F, Cha J J and Yu G H 2017 *Nano Lett.* **17** 6273–9

[88] Li H S, Peng L L, Zhu Y, Chen D H, Zhang X G and Yu G H 2016 *Energy Environ. Sci.* **9** 3399–405

[89] Liu Y Y, Merinov B V and Goddard W A 2016 *Proc. Natl. Acad. Sci. USA* **113** 3735–9

[90] Zhang J, Wang D W, Lv W, Qin L, Niu S Z, Zhang S W, Cao T F, Kang F Y and Yang Q H 2018 *Adv. Energy Mater.* **8** 1801361

[91] Cao Y L, Xiao L F, Sushko M L, Wang W, Schwenzer B, Xiao J, Nie Z M, Saraf L V, Yang Z G and Liu J 2012 *Nano Lett.* **12** 3783–7

[92] Hou H S, Banks C E, Jing M J, Zhang Y and Ji X B 2015 *Adv. Mater.* **27** 7861–6

[93] He H N, Gan Q M, Wang H Y, Xu G L, Zhang X Y, Huang D, Fu F, Tang Y G, Amine K and Shao M 2018 *Nano Energy* **44** 217–27

[94] Zhang J P, Li H H, Li Z Y, Wu X L, Zhang L L, Fan C Y, Wang H F, Li X, Wang K and Sun H Z 2016 *J. Mater. Chem.* A **4** 8242–8

[95] Xie J J, Liu L, Xia J, Zhang Y, Li M, Ouyang Y, Nie S and Wang X Y 2018 *Nano-Micro Lett.* **10** 12

[96] Yi Z, Han Q G, Geng D, Wu Y M, Cheng Y and Wang L M 2017 *J. Power Sources* **342** 861–71

[97] Zhai T, Lu X H, Ling Y C, Yu M H, Wang G M, Liu T Y, Liang C L, Tong Y X and Li Y 2014 *Adv. Mater.* **26** 5869–75

[98] Wang X F, Hu P, Chen L L, Yao Y, Kong Q Y, Cui G L, Shi S Q and Chen L Q 2017 *J. Mater. Chem.* A **5** 3839–47

[99] Deng C, Zhang S, Dong Z and Shang Y 2014 *Nano Energy* **4** 49–55

[100] Yu J, Yu Jimmy C, Ho W, Wu L and Wang X C 2004 *J. Am. Chem. Soc.* **126** 3422

[101] Bouhedja L, Steunou N, Maquet J and Livage J 2001 *J. Solid State Chem.* **162** 315–21

[102] Yabuuchi N, Kubota K, Dahbi M and Komaba S 2014 *Chem. Rev.* **114** 11636–82

[103] Pinaud B A *et al* 2013 *Energy Environ. Sci.* **6** 1983

[104] Liang L Y, Xu Y, Wang X, Wang C L, Zhou M, Fu Q, Wu M H and Lei Y 2015 *J. Power Sources* **294** 193–200

[105] Liang L Y, Liu H M and Yang W S 2013 *Nanoscale* **5** 1026–33

[106] Liang L Y, Liu H M and Yang W S 2013 *J. Alloy. Compd.* **559** 167–73

[107] He G, Li L J and Manthiram A 2015 *J. Mater. Chem.* A **3** 14750–8

[108] Zhu J, Chen L B, Xu Z and Lu B G 2015 *Nano Energy* **12** 339–46

[109] Ke L L, Dong J, Lin B, Yu T T, Wang H F, Zhang S and Deng C 2017 *Nanoscale* **9** 4183–90

[110] Xu L, Tang S, Cheng Y, Wang K Y, Liang J Y, Liu C, Cao Y C, Wei F and Mai L Q 2018 *Joule* **2** 1991–2015

[111] Hu P *et al* 2016 *Nano Lett.* **16** 1523–9

[112] Liao X B, Zhao Y L, Wang J H, Yang W, Xu L, Tian X C, Shuang Y, Owusu K A, Yan M Y and Mai L Q 2018 *Nano Res.* **11** 2083–92

[113] Tian X C, Xu X, He L, Wei Q L, Yan M Y, Xu L, Zhao Y L, Yang C C and Mai L Q 2014 *J. Power Sources* **255** 235–41

[114] Xu X, Yan M Y, Tian X C, Yang C C, Shi M Z, Wei Q L, Xu L and Mai L Q 2015 *Nano Lett.* **15** 3879–84

[115] Niu C J *et al* 2015 *Nat. Commun.* **6** 7402